energy&fuels

pubs.acs.org/EF

Article

Geochemical Impact of High-Concentration Formate Solution Injection on Rock Wettability for Enhanced Oil Recovery and Geologic Carbon Storage

Oluwafemi P. Oyenowo, Hao Wang, Abouzar Mirzaei-Paiaman, Omar A. Carrasco-Jaim, Kai Sheng, and Ryosuke Okuno*

Cite This: https://doi.org/10.1021/acs.energyfuels.3c05081

Read Online

ACCESS | Metrics & More | Article Recommendations | Supporting Information

ABSTRACT: This paper presents new data on core-scale wettability alteration of carbonate porous media with FM concentrations up to 30 wt % in NaCl brine. Experimental data from Amott tests, core floods, calcite dissolution experiments, and zeta potential measurements were analyzed to mechanistically understand the wettability alteration observed in the experiments. Static calcite dissolution tests showed that the degree of dissolution increased with increasing FM concentration in NaCl brine, even with an initially neutral pH. For example, the calcium concentration in the 30 wt % FM solution was 15.9 times greater than that in the NaCl brine with an initial pH of 7.0. Furthermore, reducing the initial solution pH from 7.0 to 6.1 for the 30 wt % FM solution caused the calcium ion concentration to increase by a factor of 3.2. Geochemical modeling and Raman analysis indicated that increased calcite dissolution was caused by interactions between calcium and FM ions. The 30 wt % FM solution with an initial pH of 6.1 yielded 4.7 times greater oil recovery than the NaCl brine in the spontaneous imbibition. The resulting Amott index indicated the wettability alteration to a water-wet state by the FM solution. The 30 wt % FM solution with an initial pH of 7.0 yielded only 30% greater oil recovery than the brine in the spontaneous imbibition; however, it reached nearly the same total oil recovery (spontaneous and forced) as the 30 wt % FM solution with an initial pH of 6.1. A numerical model was calibrated using core flood data, based on which the relative permeabilities indicated the core-scale wettability alteration by FM solutions. Results showed that increasing the FM concentration in the injection brine rendered the initially oil-wet core to a more water-wet state and that the in situ solution pH played an important role in wettability alteration by FM solution in carbonate media.

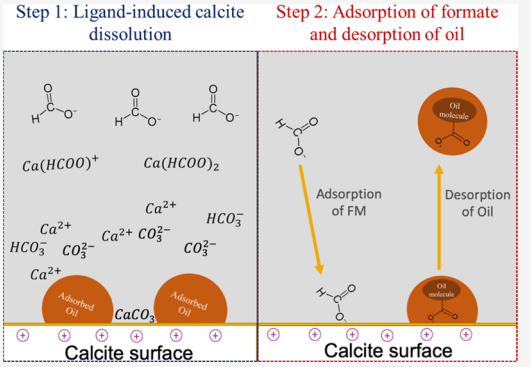

1. INTRODUCTION

The World Energy Outlook (the International Energy Agency, IEA) reported in 2022 that fossil fuels would be a significant part of the energy mix in the coming decades, accounting for over 60% of the energy mix by 2050. Oil and gas represent 75% of the fossil fuel mix.[1] Following the Paris Agreement, most countries have set greenhouse gas (GHG) reduction goals of 45% by 2030 and net zero by 2050. CO_2 emissions from burning fossil fuels accounted for 54% of global greenhouse gas emissions in 2020.[2] Hence, meeting global GHG emissions targets set by the Paris Agreement requires decreasing the carbon intensity of oil and gas production.

Carbonate reservoirs hold approximately 60% of the world's oil reserves;[3] hence, it is crucial to reduce the carbon intensity of oil production from these reservoirs. Oil recovery from carbonate reservoirs is affected by the wetting state of the rock, among many other factors. Most carbonate reservoirs are mixed/oil-wet because of the adsorption of organic components on the rock surface. Along with fracture networks often present in carbonate reservoirs, this mixed/oil-wet state tends to make conventional waterflooding without wettability alteration inefficient in improving oil recovery.[4−6]

Researchers have studied wettability modifiers that alter the wettability of carbonate rock from mixed/oil-wet to water-wet,[7−13] in which surfactants and low-salinity water (LSW) are the most widely studied. Other studies of wettability modifiers include nanofluids (nanoparticles dispersion in fluid)[14−19] and ketone solvents as polar solvents (e.g., 3-pentanone) that rapidly altered the wettability of carbonate rocks.[20−23]

The opportunity to store CO_2 and simultaneously improve oil recovery has made CO_2-assisted enhanced oil recovery (EOR) techniques increasingly popular; e.g., carbonated water injection.[24] The carbon storage associated with such CO_2-

Received: December 20, 2023
Revised: February 27, 2024
Accepted: February 29, 2024

Table 1. Mass Densities and IFTs with the Texas Crude (Table 2) for the Aqueous Solutions, and Properties of the Texas Cream Limestone Cores Used in the Amott Wettability Tests (Section 2.2)[a]

	brine case	5 wt % FM case (pH 7.0)	30 wt % FM case (pH 7.0)	30 wt % FM case (pH 6.1)
solution density, kg/m^3	980	1030	1296	1296
oleic/aqueous phase IFT, mN/m	7.37 ± 0.08	6.01 ± 0.07	2.76 ± 0.04	3.07 ± 0.08
inverse bond number	67.1	33.3	7.5	10.1
core height, cm	11.8	12.1	12.3	12.1
core diameter, cm	3.7	3.7	3.7	3.8
porosity, %	32.1	32.7	31.0	30.5
permeability, md	10.2	17.6	16.1	11.2
initial oil saturation, %	55.4	57.7	56.1	61.2
pore volume, mL	40.7	42.4	41.0	41.9
OOIP, mL	22.57	24.45	23.00	25.64

[a]The density and IFT were measured at 70°C. OOIP stands for original oil in place.

assisted EOR techniques has various shortcomings associated with inherent properties of CO_2, such as low carbon density at low to moderate pressure, low mass density, low viscosity, and corrosivity.

Aqueous formate (FM) solution can be used as a carbon carrier for geologic carbon storage.[25−28] FM ($HCOO^-$) is the simplest carboxylate and conjugate base of formic acid. Alkali FM salts such as sodium FM (HCOONa) and potassium FM (HCOOK) are highly soluble in water; for example, the solubility of potassium FM at 20 °C is 76 wt %.[29] These alkali FM salts can be produced in different ways, including from polyhydric alcohols in basic media, and catalytic conversion of carbon monoxide over sodium hydroxide.[30] An additional acidolysis process can produce formic acid (HCOOH) from these alkali FMs with additional purification and separation steps. Production of FM species is currently based on thermochemical reactions such as carbonylation of methanol and methyl FM hydrolysis, in which use of syngas and steam results in CO_2 emissions.[31,32] As an alternative, electrochemical CO_2 reduction (CO_2-ECR) can selectively produce FM species, including formic acid, using water and electricity (from renewable sources such as solar, geothermal, and wind), contributing to atmospheric carbon removal and utilization.[32−38] Analyses have demonstrated that formic acid production from electrochemical CO_2 reduction is technoeconomically feasible and environmentally sustainable. In the best scenario, the energy consumption associated with the CO_2 reduction reaction is approximately 4.5−4.7 kWh/kg HCOOH,[39,40] with estimated consumption rates of 0.95 kg CO_2/kg HCOOH and 0.60 kg H_2O/kg HCOOH.[39] Under these conditions, the overall production cost is estimated to be approximately $0.46−0.75/kg HCOOH at an industrial concentration of 85 wt %,[39,40] which is competitive with the current market price of $0.68−1/kg HCOOH.[34,39]

Numerical simulation comparisons between aqueous FM (30 wt % FM) injection and CO_2 injection into an oil reservoir showed that the FM injection resulted in 37% more carbon stored than the CO_2 injection case.[26,27] The primary reason for the enhanced carbon storage was the volumetric sweep enhanced by more stable fronts of oil and water displacement by an aqueous FM solution than by CO_2. Their cost-revenue analysis showed that CO_2 conversion into FM via ECR for FM injection was economically feasible even at current CO_2-ECR production costs, estimated based on small-scale deployments. Although no commercial CO_2 electrolyzer has been reported, accelerated progress has been made in CO_2-ECR with a current technology readiness level (TRL) of 6. For example, the carbon flux electrolyzer of 100 cm^2 produces alkali FMs from carbon dioxide and water.[41] Also, the European Commission sponsored OCEAN (Oxalic acid from CO_2 using Electrochemistry At demonstratioN scale), demonstrating the viability of the CO_2-ECR technology at an industrial scale.[42] Decades of using FM brines in drilling fluid formulations have shown that they have a favorable health, safety, and environmental profile and are compatible with oilfield equipment.[29,43] Wang et al.[28] studied the thermal stability of 20 wt % FM in a brine solution with and without calcite at 85 °C. They reported that the FM solution was stable over an aging period of 30 days and the pH of the solutions containing calcite increased due to the calcite dissolution reaction. They visually observed that calcite dissolved more in the FM solution than in brine. Baghishov et al.[7] studied carboxylate ions (FM and acetate), as wettability modifiers for carbonate rocks. The FM concentrations in their study were limited to 5 wt % sodium FM (equivalent to 3.3 wt % FM). They found that FM was more effective in altering the wettability of a carbonate core from oil/mixed-wet to water-wet when the solution pH was reduced from about 8.1 to 6.1. Their proposed mechanism of wettability alteration was that pH-induced calcite dissolution released oil from the rock surface, which was followed by the adsorption of the FM ion.

Optimizing FM solution injection for carbon storage in carbonates would require injection of high-concentration FM solutions. Increasing the FM concentration is desirable to increase the carbon density and stabilize the displacement fronts (oil and formation water) with an increased solution viscosity. However, the use of FM concentrations as high as 30 wt % would require a detailed study of the geochemical interactions and the impact on the wettability of carbonate rocks.

Therefore, this research was concerned with geochemical interactions between the FM solution and carbonate rock and the impact of the FM solution on the wettability. The effect of injecting high-concentration FM solutions (up to 30 wt %) on the carbonate rock was studied using calcite dissolution experiments, Amott wettability tests (i.e., spontaneous and forced displacements), zeta potential (ζ) measurements, and core flooding experiments. Geochemical analysis and numerical history matching of core flooding results were also performed to understand the underlying mechanisms involved in the FM injection process.

https://doi.org/10.1021/acs.energyfuels.3c05081
Energy Fuels XXXX, XXX, XXX−XXX

2. METHODS

This research consists of experimental and modeling parts. Sections 2.1 to 2.4 explain the materials and methods for the experimental part, and Section 2.5 describes the methods for numerical history matching and geochemical modeling.

2.1. Calcite Dissolution Experiments. The impact of FM concentration in brine on calcite dissolution was investigated by using different FM concentrations in NaCl brine: NaCl brine (0 wt % FM) at pH 7.0, 5 wt % FM at pH 7.0, 10 wt % FM at pH 7.0, 20 wt % FM at pH 7.0, 30 wt % FM at pH 7.0, and 30 wt % FM at pH 6.1. The FM concentration was limited to 30 wt % because it was close to the solubility limit of the sodium FM salt used in the experiment. The NaCl brine consisted of 5903 ppm of Na^+ and 9097 ppm of Cl^-. The pH values of the FM solutions were set by adding formic acid. Then, 5 g of synthetic calcite powder was added to glass vials containing 20 mL of these solutions. The mixtures were stirred and placed in an oven set at 70 °C. The supernatants from these mixtures were collected, and the pH and calcium ion concentrations in the supernatants were measured. The calcium ion concentrations were measured by using inductively coupled plasma mass spectrometry (ICP-MS). The interactions between FM and calcite in the aqueous solution were analyzed by using Raman spectroscopy. The ζ of the calcite−water interface in the NaCl brine, 30 wt % FM at pH 7.0, and 30 wt % FM at pH 6.1 solutions were measured to understand the effect of FM and pH on the calcite surface charge.

Also, the effect of pressure on calcite dissolution by FM solution was tested using an Iceland spar calcite chip (from Ward's Science) and the 30 wt % FM solution at pH 7.0, at 70 °C. At every 500 psi pressure step, the system pressure was maintained for 24 h to allow the system to equilibrate before collecting a sample solution from the system. The calcium concentration in the solution was then measured by using ICP-MS.

2.2. Amott Wettability Tests. Amott wettability tests, consisting of spontaneous and forced displacements, were performed by using Texas Cream limestone cores. Four aqueous solutions were selected out of the six solutions mentioned in Section 2.1. Table 1 lists the mass densities for the four solutions: NaCl brine, 5 wt % FM solution at pH 7.0, 30 wt % FM solution at pH 7.0, and 30 wt % FM solution at pH 6.1. The pH values refer to the initial solution pH, which varied during the experiments. Table 1 also gives the interfacial tension (IFT) values measured for the aqueous solutions with the oil used for the experiment (Table 2), and the core properties measured in this research.

Table 2. Oil Composition and Properties

components	mass percent
C_3	0.1%
C_4	0.4%
C_5	1.5%
C_6	3.0%
C_7	4.8%
C_8	6.5%
C_9	5.6%
C_{10}	5.2%
C_{11}	4.1%
C_{12}	4.0%
C_{13}	4.1%
C_{14}	3.7%
C_{15+}	57.0%
relative molecular weight, g/mol	183
density, kg/m^3	795 (at 22 °C)
	770 (at 70 °C)
viscosity, cp	2.7 (at 22 °C)
oil/DI water IFT, mN/m	19.75 (at 22 °C)

The cores were initially saturated with brine and then with oil at room temperature. The cores were then aged in oil for 12 weeks (6 weeks at 70 °C followed by 6 weeks at room temperature). Subsequently, the oil was injected again into the cores to achieve a more uniform fluid distribution and to ensure that the cores were at their residual water saturation.

2.2.1. Spontaneous Imbibition. The solutions to be tested were prepared and placed in an oven, set at 70 °C (the experiment temperature), for 24 h. The oil-saturated cores were placed in the Amott cells, which contained the respective solutions. To minimize the effect of fluid expansion, both the cells and the solutions were set up at 70 °C. Amott cells were placed in the oven at 70 °C for the duration of the experiment. The oil recovery was recorded periodically by measuring the amount of oil collected at the top of the Amott cell. The calcium ion concentrations in the solutions after spontaneous imbibition were measured by using ICP-MS.

2.2.2. Forced Imbibition. After spontaneous imbibition, the cores underwent forced oil displacement by the respective aqueous solution. Figure 1 shows a schematic of the experimental setup used. The setup

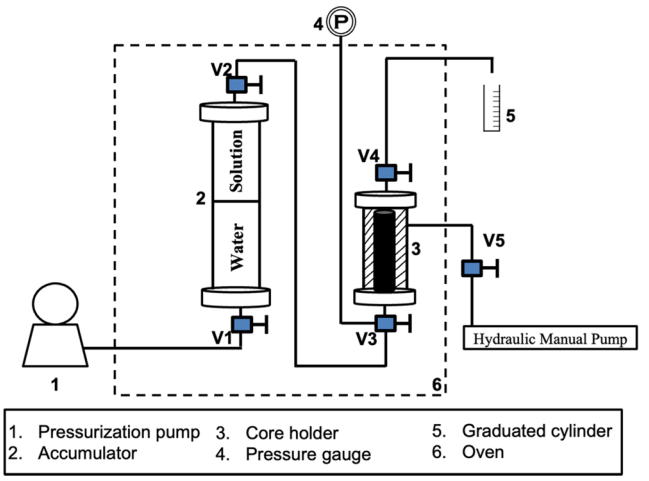

Figure 1. Schematic for the experimental setup for the forced imbibition (Section 2.2.2)

consisted of a pressurization pump (Teledyne ISCO 100 DX), a hydraulic pressure pump (ENERPAC P-391) to provide overburden pressure, an accumulator for the injection solution, a Hassler-type core holder, 2-way valves, and an oven for maintaining the system temperature at 70 °C.

Core flooding was started by injection of the respective solution at a constant rate of 40 mL/h. The injection rate was set such that the critical capillary number of 2×10^{-5} was not exceeded, as explained in the next section. The capillary number, N_{vc}, is the dimensionless ratio of viscous to capillary forces. The most fundamental form of capillary number is

$$N_{vc} = \frac{K\Delta P}{\sigma L} \tag{1}$$

where K is permeability, ΔP is the differential pressure across the flow distance (L), and σ is the oil/water interfacial tension.[44]

After the water cut reached 100%, the injection flow rate was increased from 40 to 200 mL/h to minimize the capillary end effect on the final fluid saturations. The injection rate was increased such that the Rapoport and Leas number N_{RL} of 3 cP-cm^2/min was exceeded[44,45]

$$N_{RL} = Lv\mu \tag{2}$$

where L is the length of the core in centimeters, v is the superficial velocity in cm/min, and μ is the injected fluid viscosity in cp. The produced fluids were collected in graduated vials to calculate the oil recovery.

https://doi.org/10.1021/acs.energyfuels.3c05081
Energy Fuels XXXX, XXX, XXX−XXX

2.3. Core Flooding. Indiana limestone cores were used for the core flood experiments. The cores were 2.54 cm in diameter and 22.86 cm in length. The porosities and permeabilities of the cores were measured with brine in the core flood system. Then, oil was injected into the core to establish the initial oil saturation, which was calculated by the produced brine volume. During the oil injection process, the pressure drop was measured using a pressure transducer to estimate the end-point relative permeability of the oil.

Core floods were performed with brine, 20 wt % FM, and 30 wt % FM solutions at room temperature with all initial pH values of 7.0. Table 3 summarizes the experimental conditions. The viscosity ratio

Table 3. Experimental Conditions for Core Flooding Tests with Indiana Limestone Cores

experiment	brine case (pH 7)	20 wt % FM case (pH 7)	30 wt % FM case (pH 7)
porosity, %	22.07	22.36	21.58
permeability, mD	44.66	53.24	45.57
pore volume, mL	25.56	25.90	25.00
initial oil saturation, %	50.86	52.42	52.05
viscosity of injected fluid, cp	1.0	3.3	8.3
viscosity ratio	2.70	0.82	0.33
injection rate, mL/h	12.00	3.64	1.45
capillary number	6.47×10^{-7}	3.02×10^{-6}	2.04×10^{-6}

shown in Table 3 is the ratio of the viscosity of oil to that of the injection fluid. The injection rate was designed based on the capillary number. Though the brine case had a flow rate higher than that of the FM solution cases, its capillary number was lower because it had a greater oil/aqueous phase IFT and a smaller viscosity than the FM solutions. According to Lake et al.,[44] the residual oil saturation is independent of capillary number at a low capillary number; however, the residual oil saturation begins to decrease when the capillary number is above the critical capillary number. In this experiment, therefore, a low capillary number was designed for all three core floods. Injection rates for FM cases were smaller than the brine case because of the viscosity of FM solution being higher than that of brine. The fluids were injected for about 1.5 pore volumes. The effluent samples were collected in plastic graduated vials. The volumes of the oil and water phases were measured to calculate the oil recovery.

Results of core flooding tests were history-matched by numerical simulation to quantify the wettability alteration using the calibrated relative permeabilities, as explained in Section 2.5.2. Note that the FM solutions were more viscous than the brine as shown in Table 3, leading to an increased displacement efficiency according to the Buckley-Leverett theory.[27]

2.4. Material Analysis. *2.4.1. Ion Concentration Measurement Via ICP-MS.* The calcium concentration in solution was determined using an Agilent 7500ce ICP-MS. ICP-MS is an analytical technique used for determining elemental composition. It uses a coupled argon plasma to ionize the solution using a torch, and the resulting ions are measured with a mass analyzer, usually a quadrupole. The spectra produced consist of isotope peaks for each element present. These spectra are used to identify the elements and for their quantitative determination based on calibration curves. Before analysis, the solution was diluted using nitric acid (2%v/v) until total dissolved solids (TDS) $\leq$ 200 ppm. The instrument was optimized for sensitivity across the atomic mass unit (AMU) range, while minimizing oxide production (<1.05%). The quantitative analytical method employed an octupole reaction system (ORS), operated in helium (collision-mode) and hydrogen (reaction-mode) for the removal of polyatomic interferences. Internal standards, mixed into unknowns via in-run pumping, were used to compensate for instrumental drift and internal standard sensitivity variations were well within quality assurance tolerances (±20%).

2.4.2. Zeta Potential Measurement. Suspensions of calcite in solution were prepared using synthetic calcite powder; 10 g of calcite powder was added to 250 mL of solution. The ζ of each suspension was then measured by using the ZetaProbe (Colloidal Dynamics, LLC). The ZetaProbe operates by generating electrokinetic sonic amplitude (ESA) signals, which is an application of electroacoustics. The instrument uses ESA to calculate the ζ. To determine the ζ values of the particles, the ESA signal of the background electrolyte was measured and adjusted by the instrument in the ζ determination of the suspensions. The measurements were done while stirring the suspensions at 400 rpm and 22.5 °C.

2.4.3. Powder X-ray Diffraction (XRD). XRD is a nondestructive technique for determining the crystal structure of a material, allowing for chemical identification. XRD was used to characterize the solid residue from the FM and calcite reaction. The solid residue was dried in an oven at 75 °C. The crystal structure of the solid residue was characterized by XRD utilizing a Rigaku Miniflex 600 diffractometer with Cu Kα radiation (λ = 1.5405 Å). The scan axis, 2θ, was set to start at 0° and stop at 80° with a step size of 0.04° and a speed of 4.0°/min.

2.4.4. Raman Spectroscopy. Raman spectroscopy is a technique for analyzing quantified vibrational changes within a sample. Raman spectroscopy is based on the principle of inelastic scattering of light in which the visible wavelength of a small fraction of the radiation scattered by certain molecules differs from the energy of the incident beam (monochromatic laser in the visible or near-IR spectral region). The difference in wavelength between the incident and the scattered radiation provides information on the chemical structure of the molecules.[46] Raman spectroscopy was used to examine the vibrational, rotational, and low-frequency modes of FM in the presence of calcite. A 1 mL aliquot was taken from the solution after the reaction between FM and calcite was completed and placed in the sample holder. Raman spectra were obtained using a Witec Micro-Raman Spectrometer α 300, with a laser wavelength of 532 nm and 7 mW power. The spectral integration time was set to 1 s. The instrument was routinely checked by using graphene to ensure proper operations.

2.4.5. IFT Measurement. The oil/aqueous phase IFT at room temperature was measured using a ramé-hart model 500 advanced goniometer/tensiometer along with the DROPimage Advanced software for drop shape analysis. The pendant drop method was used for IFT determination at room temperature. The IFT was calculated from the drop shape analysis and density difference by fitting the Young−Laplace equation. For oil/aqueous phase IFT measurements at 70 °C, a Kruss Scientific spinning drop tensiometer was used.

2.5. Simulation and Modeling. *2.5.1. Geochemistry Modeling Using PHREEQC.* Geochemical reaction models in the PHREEQC software[47] were used to mechanistically understand the interactions between the FM solution and calcite. PHREEQC can simulate dissolution reactions of minerals in aqueous solutions by employing equilibrium chemistry principles.

The solubility of a mineral in a solution is expressed as a mass-action equation with a temperature-dependent equilibrium constant. For example, the dissolution of calcite is written as $CaCO_{3\,(s)} \rightarrow Ca^{2+}_{(aq)} + CO^{2-}_{3\,(aq)}$ with the equilibrium constant $\log_{10} K_{25\,°C} = -8.48$. The resulting mass-action expression is

$$K_{25\,°C} = 10^{-8.48} = \frac{a_{Ca^{2+}} a_{CO_3^{2-}}}{a_{CaCo_3}} \quad (3)$$

where a_x is the activity of component x in solution. The activity, a_x, is defined as the product of the molar concentration of component x and the activity coefficient of component x in solution. The activity of a pure solid is 1.0 by convention.

PHREEQC uses the mass-action equation for solubility to model the ionic concentrations based on the activity coefficient of the ions and the properties of the solution. In this research, the compositions of the aqueous solutions were defined and used as inputs in the equilibrium models. Then, PHREEQC estimated the activity of each

https://doi.org/10.1021/acs.energyfuels.3c05081
Energy Fuels XXXX, XXX, XXX−XXX

Table 4. Reactions Included in the Geochemical Model (Section 2.4.1)[a]

	reaction	$\log_{10} K_{25\,°C}$	$\Delta H_{25\,°C}$ (kJ/mol)	data source
A1	$H^+ + CO_3^{2-} \Leftrightarrow HCO_3^-$	10.330	−14.700	Sit.dat
A2	$2H^+ + CO_3^{2-} - H_2O \Leftrightarrow CO_2$	16.680	−23.860	Sit.dat
A3	$Na^+ + H^+ + CO_3^{2-} \Leftrightarrow NaHCO_3$	10.080	−26.127	Sit.dat
A4	$Na^+ + CO_3^{2-} \Leftrightarrow Na(CO_3)^-$	1.270	37.279	Sit.dat
A5	$Na^+ + Cl^- \Leftrightarrow NaCl$	−0.500	2.000	Sit.dat
A6	$Ca^{2+} + CO_3^{2-} \Leftrightarrow CaCO_3$	3.220	14.830	Sit.dat
A7	$Ca^{2+} + H^+ + CO_3^{2-} \Leftrightarrow Ca(HCO_3)^+$	11.430	−23.597	Sit.dat
A8	$Ca^{2+} + Cl^- \Leftrightarrow CaCl^+$	−0.290	7.150	Sit.dat
A9	$Ca^{2+} + 2Cl^- \Leftrightarrow CaCl_2$	−0.640	−5.858	Sit.dat
A10	$Ca^{2+} - H^+ + H_2O \Leftrightarrow Ca(OH)^+$	−12.780	77.206	Sit.dat
A11	$H^+ + Cl^- \Leftrightarrow HCl$	−0.710	−12.298	Sit.dat
A12	$H^+ + FM^- \Leftrightarrow H(FM)$	3.745	0.167	Minteq.v4.dat
A13	$Na^+ + FM^- \Leftrightarrow Na(FM)$	0.117	−1.325	Shock and Koretsky;[57] Anderson[101]
A14	$Na^+ + 2FM^- \Leftrightarrow Na(FM)_2^-$	−0.122	−13.206	Shock and Koretsky;[57] Anderson[101]
A15	$Ca^{2+} + FM^- \Leftrightarrow Ca(FM)^+$	1.430	−3.079	Shock and Koretsky;[57] Anderson[101]
A16	$Ca^{2+} + 2FM^- \Leftrightarrow Ca(FM)_2^0$	2.309	−9.099	Shock and Koretsky;[57] Anderson[101]
M1	$Ca(FM)_2 \Leftrightarrow Ca^{2+} + 2FM^-$	−0.760	7.088	Loos et al.;[53] Wagman et al.[102]
M2	$CaCO_3 \Leftrightarrow Ca^{2+} + CO_3^{2-}$	−8.480	−10.620	Sit.dat

[a]A: aqueous phase reactions, M: mineral dissolution reactions.

ion in the solution using the selected activity coefficient model and interaction parameters.

The activities of ions in solution depend on long-range electrostatic forces and short-range interionic forces within the solution. Ions in solution form complexes with each other, which affect the activity of the ions.[48] Accurate estimation of the activity coefficient by PHREEQC requires a comprehensive description of reactions in the bulk aqueous phase (including ion complexation) and an appropriate activity coefficient model.

PHREEQC has two models that account for short-range and nonelectrostatic interactions, which are important in highly concentrated solutions. These are the Pitzer model contained in the pitzer.dat database and the specific ion interaction theory (SIT) model contained in the sit.dat database. The Pitzer equation is a rigorous model that describes the ionic interactions in solutions; however, it requires several ion-specific interaction parameters, which are not currently available for FM ions.[49] For this research, therefore, a simpler SIT activity coefficient model was implemented by using the sit.dat database in PHREEQC. The SIT model for the activity coefficient, γ_i, of an ion of charge z_i in solution is given as

$$\log_{10} \gamma_i = -z_i^2 \frac{A\sqrt{I}}{1 + b\sqrt{I}} + \sum_k \varepsilon(i, k) m_k \quad (4)$$

where A is the limiting Debye−Hückel slope, b is an empirical constant, I is the ionic strength of the solution, $\varepsilon(i,k)$ is the interaction coefficient between ion i and an opposite charged ion, k, and m_k is the molality of the ion k. The original SIT model assumes that the interaction coefficients are constant and independent of the ionic strength. However, Bretti et al.[50] found the interaction coefficient to be a function of ionic strength, and proposed a new equation for the estimation of ε as

$$\varepsilon = \varepsilon_\infty + \frac{\varepsilon_0 - \varepsilon_\infty}{I + 1} \quad (5)$$

This modified equation was used for calculating ε for the Na/Ca-FM interactions. Values of ε_∞ and ε_0 for sodium FM were obtained from Bretti et al.[51] The ε value for calcium FM was calculated using a regression model provided by Crea et al.[52] and data from Loos et al.[53]

Calcium and sodium can form both unidentate and bidentate complexes with FM.[54−56] The chemical equations for the formation of the FM complexes were added to the model for a better description of the aqueous system. Thermodynamic data (standard Gibbs free energy of formation and standard enthalpy of formation) for the FM complexes were taken from Shock and Koretsky,[57] and PHREEQC databases. All of the reactions considered in the geochemical model and their respective data sources are defined in Table 4.

The dissolution of calcite leads to the formation of CO_2. Because the vials used in the calcite dissolution experiment were closed, the CO_2 pressure in the vials should not be the partial pressure in air at atmospheric pressure. Since the activity coefficient model is accurate at low concentrations, we estimated the CO_2 partial pressure by matching the measured calcium ion concentration in brine and assumed that the CO_2 partial pressure was the same for all other solutions. After the calibration was done, the model was used to estimate the calcium ion concentrations in the FM solutions and compared with the measured concentrations from the calcium dissolution experiment (see the Supporting Information for the PHREEQC input script).

2.5.2. History Matching of Core Flooding Tests. Core flooding results were numerically history-matched using CMG IMEX.[58] Using either mercury injection capillary pressure (MICP) or imaging techniques, Alarji et al.,[59] Churcher et al.,[60] Elkhoury et al.,[61] and Lipovetsky et al.[62] performed pore structure analyses on Indiana limestone cores and reported that the pore size distribution was bimodal. Hence, our numerical simulation model consisted of two parallel layers with different permeabilities (higher and lower) and cross-sectional areas, which yielded additional flexibility in the history matching. No cross-flow was considered between the two layers.

The history matching consisted of two steps. The first step was to adjust the permeability and area for each layer to match the oil recovery before the water breakthrough. The heterogeneity of the simulation model significantly affects the first breakthrough time and

https://doi.org/10.1021/acs.energyfuels.3c05081
Energy Fuels XXXX, XXX, XXX−XXX

the oil recovery history. The average permeabilities of the cores were measured by brine before the core flood experiments. Hence, during the first step of the history matching, the permeability and area of the two layers were adjusted subject to the following

$$K_{average} = K_1A_1 + K_2A_2 \quad (6)$$

where $K_{average}$ is the measured average permeability, K_i is the permeability of each layer (1 for high permeability and 2 for low permeability), and A is the area ratio of each layer to the total cross section of the core. After adjustment, the flow capacity ratio (i.e., K_1A_1/K_2A_2) was fixed at 17 for the three models to maintain the same tendency for channeling flow at the core scale.

The second step was to adjust the relative permeability curves by matching the oil recovery behavior after the water breakthrough. The end-point relative permeability of oil was estimated from the core flooding experiments to be 0.408 and was fixed at this value for the three models. The residual oil saturation and irreducible water saturation were also determined from the core flooding experiments. The end-point relative permeabilities of water, water exponent, and oil exponent were adjusted to further match the second water breakthrough and oil recovery. Table 5 shows the simulation settings

Table 5. Parameters for Two Layers in the History Matching of Core Flooding Results (Section 2.5.2)[a]

	K_1A_1/K_2A_2	K_1, mD	A_1, area %	K_2, mD	average K, mD
brine	17	55	76.0	11	45
20 wt % FM	17	57	88.7	26	53
30 wt % FM	17	46	97.3	39	46

[a]The three solutions had an initial pH of 7.0.

and parameters for each solution injection model after history matching. In the simulation model, the aqueous phase viscosity was based on experimentally measured data for FM solutions[28] and was therefore not adjusted in the history matching.

Finally, the wettability alteration by FM was quantified using the Lak wettability index and modified Lak wettability index. The Lak wettability index is defined as[63]

$$I_L = \frac{A(0.3 - k_{rw,Sor})}{0.3} + \frac{B(0.5 - k_{rw,Sor})}{0.5} + \frac{CS - RCS}{1 - S_{or} - S_{wc}} \quad (7)$$

where I_L is the Lak wettability index, which ranges from −1.0 to 1.0, where −1.0 and 1.0 indicate strongly oil-wet and strongly water-wet, respectively; $k_{rw,\ Sor}$ is the water relative permeability at residual oil saturation; CS is the intersection saturation point of oil and water relative permeability curves; and RCS is the reference crossover saturation defined as

$$RCS = 0.5 + \frac{S_{wc} - S_{or}}{2} \quad (8)$$

S_{or} and S_{wc} are the residual oil saturation and irreducible water saturation, respectively, and A and B are two coefficients defined as

$$A = 0.5 \text{ and } B = 0.0, \text{ if } k_{rw,Sor} < 0.3$$

$$A = 0.0 \text{ and } B = 0.0, \text{ if } 0.3 \le k_{rw,Sor} \le 0.5$$

$$A = 0.0 \text{ and } B = 0.5, \text{ if } k_{rw,Sor} > 0.5$$

We note that to use the Lak wettability index, relative permeability is defined as effective permeability divided by oil permeability at initial water saturation.

Modified Lak wettability index is defined as[64]

$$I_{ML} = \frac{A_o - A_w}{A_o + A_w} \quad (9)$$

where I_{ML} is the modified Lak wettability index, and A_o and A_w are the areas below the oil and water relative permeability curves, respectively.

Baghishov et al.[7] provided FM adsorption data for Texas Cream limestone. They recorded that 0.11 mg of FM was adsorbed per gram of Texas Cream limestone. Although the core floods in this research were conducted on Indiana limestone cores (not Texas Cream limestone), we used the measured adsorption data to perform preliminary simulations of the effect of adsorption. Preliminary simulations using the adsorption value showed that adsorption did not significantly impact the simulated oil recovery. This was because the adsorption capacity of the core was small compared with the injected FM concentration. Hence, the current simulation model without FM adsorption is reasonable.

3. RESULTS

This section presents results from the experiments described in the previous section. A mechanistic analysis is given to the wettability alteration observed in the core-scale experiments such as Amott wettability tests and core flooding.

3.1. Calcite Dissolution Measurements and Geochemical Simulation. Figure 2 shows the calcite level in the tested FM solutions at different concentrations after 24 h. The calcite powder level decreased as the FM concentration increased up to 30 wt %. From this observation, the presence of FM in solution favored calcium carbonate dissolution. We hypothesized that the dissolution followed the chemical equation:

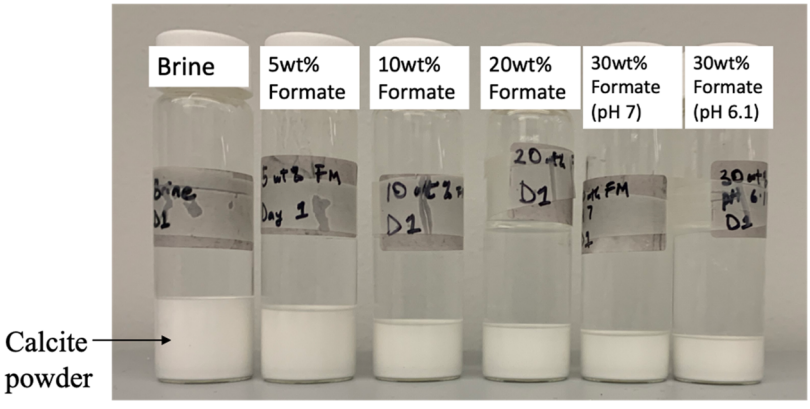

Figure 2. Snapshot of the calcite dissolution experiment in different aqueous solutions after 24 h. All experiments were initiated using 20 mL of aqueous solution and 5 g of synthetic calcite. The calcite level reduced with increasing FM concentration.

https://doi.org/10.1021/acs.energyfuels.3c05081
Energy Fuels XXXX, XXX, XXX−XXX

$$CaCO_{3(s)} + 2NaHCOO_{(aq)} + H_2O_{(l)} + CO_{2(g)} \leftrightarrow Ca(HCOO)_{2(aq)} + 2NaHCO_{3(aq)}$$

Figure 3 shows the calcium ion measurements from the calcite dissolution experiment. At the initial stage, the calcite dissolution was slowly driven by the equilibrium between H_2O (from brine) and CO_2 (from the air), where a small amount of Ca^{2+} and HCO_3^- ions were released. This is consistent with the brine result in Figure 4, which shows the averages of the measured calcium concentrations from Figure 3. The brine used in preparing the FM solution did not contain any calcium ions; hence, any calcium ion in the solution was from dissolved calcite.

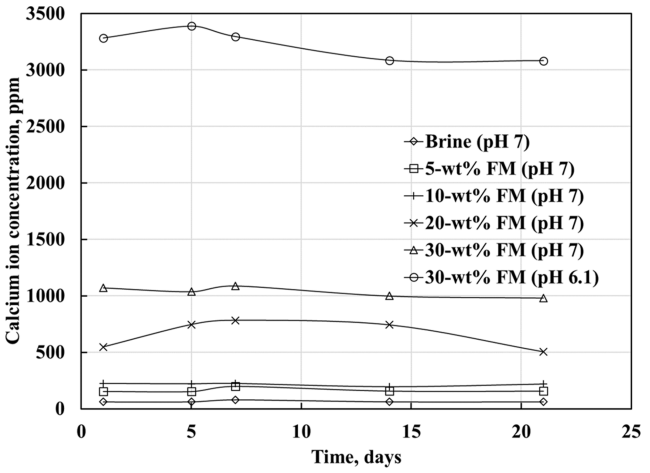

Figure 3. Calcium ion concentrations measured for different aqueous solutions after aging with calcite (Section 3.1). Calcite dissolution reached an equilibrium state rapidly with small variations after 1 day.

In the presence of NaHCOO, an ion exchange reaction between the dissolved Ca^{2+} ions and the dissociated $HCOO^-$ ions occurred, allowing the formation of the calcium biformate $[Ca(HCOO)_2]$ as a product in the solution. As the FM concentration increased, the reaction equilibrium allowed more calcite dissolution to compensate for the Ca^{2+} concentration difference with respect to FM ions. This effect was observed in Figure 4, where a greater concentration of Ca^{2+} was detected in the solution as the FM concentration increased. Notably, FM addition led to rapid calcite dissolution, mostly within 1 day, as shown in Figure 3.

Further analysis of the FM ion interaction within the calcite dissolution was performed by Raman characterization (Figure 5). A sample of the 30 wt % sodium FM in brine solution was used as a reference (labeled as NaFM brine), as shown in Figure 5a. The observed bands were assigned to the characteristic vibration modes of the FM molecule.[65] The bands related to the C−H modes are at 1085, 1383, and 2732−2822 cm^{-1}, which corresponded to out-of-plane deformation, in-plane deformation, and stretching vibrations, respectively. In addition, the bands located at 763 and 1351 cm^{-1} are associated with the O−C−O scissor mode and C−O symmetric stretching. The broad peak centered at 3442 cm^{-1} is related to the strong O−H stretching band of water.[65]

In the case of a reaction sample composed of $CaCO_3$ + NaFM brine, the bands assigned to O−C−O scissor mode vibration and the C−H out-of-plane deformation are not present in the FM molecule response because of the interaction with the released ions from calcite dissolution, which might be creating a steric hindrance environment for the vibrations. This effect is well observed in Figure 5b, in which the vibrations of C−O and C−H bonds at 1354 and 1380 cm^{-1} are shifted toward higher frequencies in the presence of calcite dissolution (1355 and 1386 cm^{-1}, respectively). This behavior can be associated with the differences in the cation sizes and their coordination numbers over the vibrational modes of the FM molecule, affecting the Ca^{2+}−O and Na−O bond lengths and allowing a certain degree of distortion.[66,67] Thus, it is evident that the interaction between FM and Ca^{2+} to

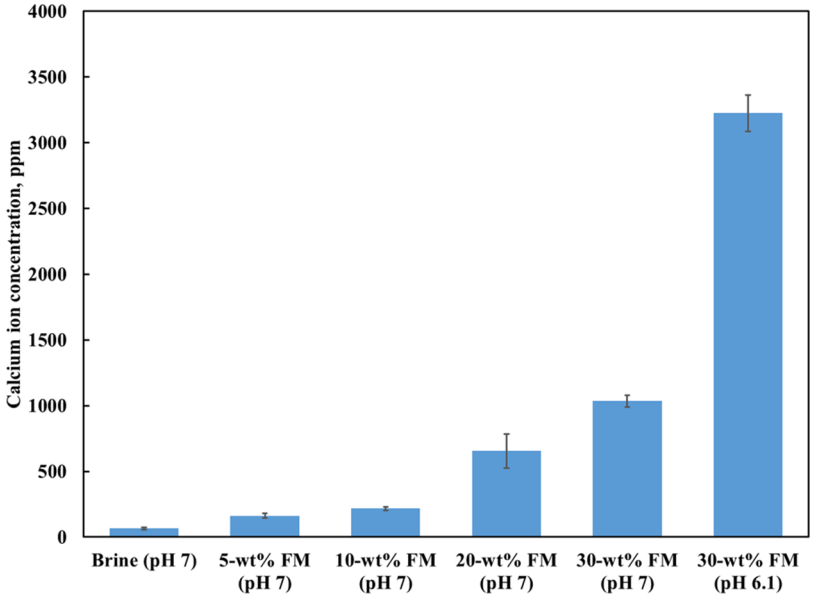

Figure 4. Average calcium ion concentrations after the calcite dissolution experiment (Section 3.1). It is an average of the measurements shown in Figure 3. Increasing the FM concentration increased the calcium ion concentration for an initially neutral pH. Changing the pH of the 30 wt % FM solution had a significant effect on the calcite dissolution.

https://doi.org/10.1021/acs.energyfuels.3c05081
Energy Fuels XXXX, XXX, XXX−XXX

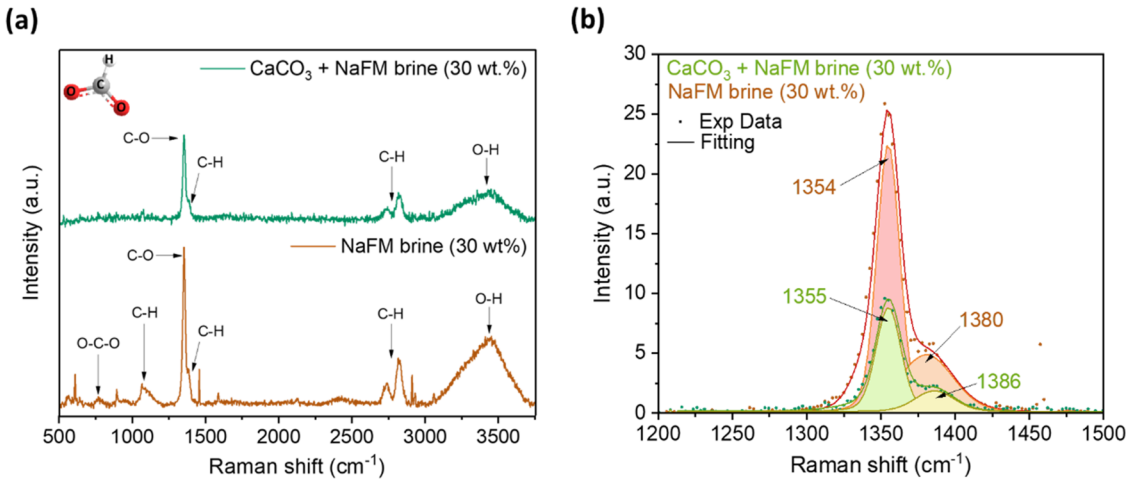

Figure 5. Raman spectra of 30 wt % sodium FM in brine solution (labeled as NaFM brine) and $CaCO_3$ + NaFM brine (Section 3.1); full spectra comparison (a), and peak deconvolution (b).

produce calcium biformate by the ion exchange reaction led to an enhanced level of calcite dissolution.

An additional key parameter is the effect of the initial pH in the NaFM + brine solution. Comparisons between the two 30 wt % FM solutions indicate that reducing the initial solution pH from 7.0 to 6.1 caused the calcium ion concentration to increase by a factor of 3.2. This can be associated with the increment in the initial H_2CO_3 concentration from the CO_2 and H_2O reaction, which favors calcite dissolution.

The pH profile of the two 30 wt % FM solutions (Figure 6) shows that the two solutions approached a similar equilibrium

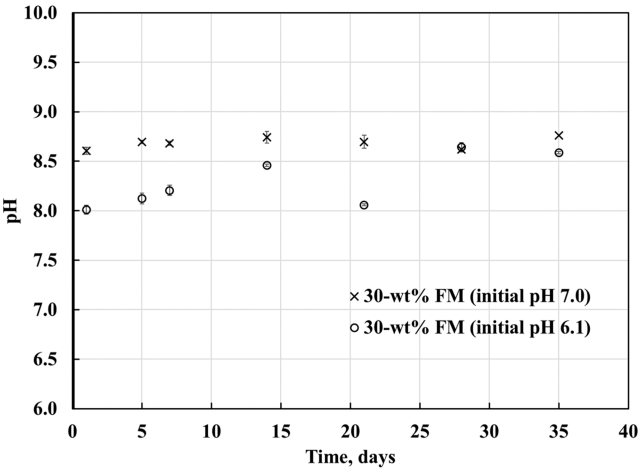

Figure 6. pH histories of the 30 wt % FM solutions after the calcite dissolution experiment. Both solutions had a similar equilibrium pH; however, the 30 wt % FM with an initial pH of 6.1 took longer to reach the equilibrium pH.

pH with time, although the 30 wt % FM (pH 6.1) solution took a longer time to reach the equilibrium pH. The FM/formic acid mixture is a well-known pH buffer. The strength of the buffer increases as the pH approaches the negative logarithm of the formic acid dissociation constant, pK_a, of 3.75. Therefore, the 30 wt % FM with an initial pH of 6.1 would resist changes in pH more strongly than the 30 wt % FM with an initial pH of 7.0. This buffer strength of 30 wt % FM solution with an initial pH of 6.1 explains the slower rise in pH in Figure 6.

After the reaction, XRD analysis (Figure 7) of the solid residue from the 30 wt % FM (pH 6.1) solution showed the

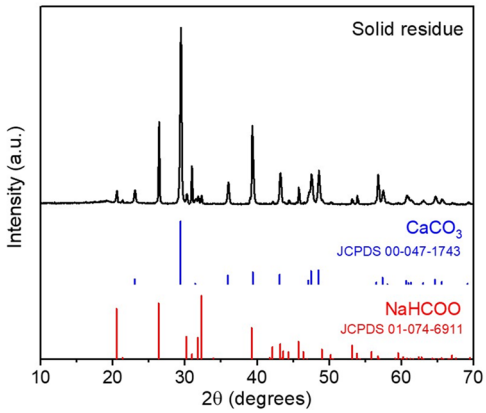

Figure 7. XRD pattern of the solid residue from the 30 wt % FM (pH 6.1) solution (Section 3.1). The JCPDS reference indexes for the identified phases are shown in the figure.

minerals present were $CaCO_3$ and NaHCOO, with no evidence of an additional phase that might have affected the measured calcium concentrations. The sodium FM crystals were likely deposited on calcite during the drying process.

The effect of the pressure on the calcite dissolution by FM was studied by calcite dissolution experiments at different pressures. The calcium concentration was measured to be 863.2 at 21.7 psia, 1090.2 at 502.7 psia, 927.7 at 1002.7 psia, 830.2 at 1502.7 psia, and 921.5 at 2002.7 psia. The results show that the calcite dissolution by FM was not significantly affected by the pressure. Figure 8 compares the calcium ion concentrations measured from the calcite dissolution experiment and the PHREEQC geochemical model. The model was in good agreement with the experimental data except for the 30 wt % FM at an initial pH of 6.1. The substantial deviation observed for this solution likely came from the elevated level of calcite dissolution and the involved reactions.

An initial attempt to investigate the deviation for the 30 wt % FM solution (pH 6.1) was to back-calculate the CO_2 partial pressure that matches the calcium concentration data. Because the systems were closed, it is conceivable that the partial

https://doi.org/10.1021/acs.energyfuels.3c05081
Energy Fuels XXXX, XXX, XXX−XXX

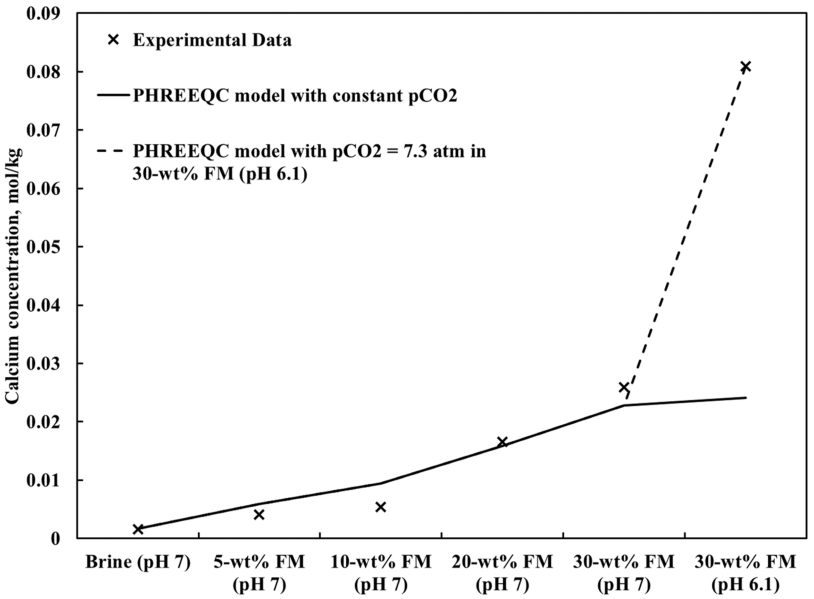

Figure 8. Calcium ion concentrations from PHREEQC and measurements using ICP-MS (Section 3.1). The PHREEC model assuming a constant partial pressure of CO_2 (pCO_2) gave a good match for all solutions except for the 30 wt % FM solution with an initial pH of 6.1. Increasing pCO_2 to 7.3 atm for the 30 wt % FM solution with an initial pH of 6.1 gave a good match with the data; however, such a large pCO_2 was unrealistic. The deviation comes likely from a combination of the assumed pCO_2 and inaccurate estimate of activity coefficients.

pressure of the CO_2 increased with an increased amount of dissolved calcite. However, matching the calcite concentration in the 30 wt % FM (pH 6.1) required the CO_2 partial pressure for the 30 wt % FM solution (pH 6.1) to increase to 7.3 atm, which is unrealistically large. Therefore, the CO_2 partial pressure alone does not explain the deviation observed for this solution in Figure 8.

Another potential reason for the inaccurate result for the 30 wt % FM solution (pH 6.1) in Figure 8 is that the activity coefficient model could not describe the effect of hydrogen ion activity on ionic interactions in the solution, leading to inaccurate estimations of the aqueous species activity coefficients. A more detailed description of the FM solution and its ionic interactions is necessary to accurately describe highly concentrated FM solutions. The development of such models, although beyond the scope of this study, will be important for modeling aqueous FM solutions at high concentrations.

The results from Raman analysis and the model indicate that the increased level of calcite dissolution by FM occurred because of the interactions between Ca^{2+} and FM ions. The aqueous speciation in PHREEQC showed that calcium in the solution existed predominantly (approximately 90%) as $CaHCOO_{(aq)}^{+}$ and $Ca(HCOO)_{2\,(aq)}$ complexes, whereas the dissolved carbonates were predominantly present as $HCO_{3(aq)}^{-}$, $NaHCO_{3\,(aq)}$, and $Na(CO_3)_{(aq)}^{-}$. These carbonate species were also present in the brine solution, although the relative concentrations of the $Na(CO_3)_{(aq)}^{-}$ and $NaHCO_{3\,(aq)}$ increased with increasing sodium FM concentration because of the increased Na concentration. The impact of the FM ion was shown in the formation of the calcium and FM complexes. These calcium and FM complexes reduce the activity coefficient of the calcium ion, consequently increasing the molar concentration of dissolved calcite.

Although no secondary phase precipitations were observed during the calcite dissolution experiment, it was important to track the saturation index for possible minerals in the solution. The saturation index (SI) is a measure of the degree of saturation of a solution with respect to a mineral. The SI was calculated by comparing the activities of dissolved mineral ions to the solubility product of the mineral, for example, $SI_{gypsum} = \log_{10} \frac{a_{Ca^{2+}} \times a_{SO_4^{2-}}}{Ksp_{gypsum(CaSO_4)}}$. SI of 0 indicates that the solution is saturated with a mineral, a negative SI indicates undersaturation, and an SI greater than 0 indicates supersaturation (and possible precipitation). PHREEQC calculated the SI values of all possible minerals (including polymorphs) that can be formed from a combination of elements in solution. In this paper, we restricted our analysis to minerals with SI values greater than −5. Figure 9 shows the saturation index for different minerals calculated from the geochemical model. All of the solutions were saturated with calcite (i.e., $SI_{calcite} = 0$) and were not included in the plot because it was part of the model setting. None of the minerals had an SI greater than 0,

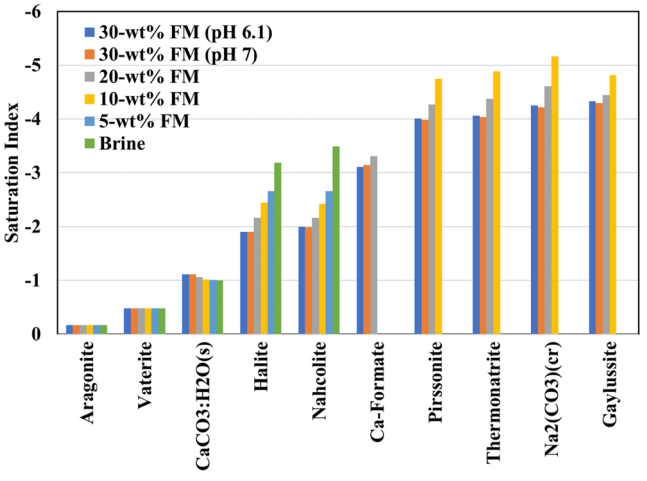

Figure 9. Saturation indexes of minerals calculated from the geochemical model (Section 3.1).

https://doi.org/10.1021/acs.energyfuels.3c05081
Energy Fuels XXXX, XXX, XXX−XXX

which is in agreement with the XRD analysis of the solid residue from the calcite dissolution experiment. Aragonite, vaterite, and $CaCO_3.H_2O$ (monohydrocalcite) had the largest SI of the minerals considered. Aragonite, vaterite, and monohydrocalcite are all forms of calcite, and since the solution was saturated with calcite, it is reasonable for their SI to be most significant. Despite the abundance of the FM ions in solution, the SI of the calcium FM mineral was less than −3 in all of the solutions, thus making precipitation of the salt unlikely. The next sections will address a question as to how the elevated level of calcite dissolution affected the static and dynamic core-scale experiments, Amott tests and core flooding, in this research.

3.2. Amott Test. Figure 10 shows the oil recoveries from spontaneous imbibition experiments. The data were scaled using the Leverett radius, $\sqrt{K/\phi}$, to account for differences in the pore structure among the different cores used.[68−70] The 30 wt % FM solution with an initial pH of 6.1 yielded the highest oil recovery, 23% pore volume (PV), which was much greater than the other solutions tested. The oil recoveries from the other three solutions were 5.3, 6.1, and 6.8% PV for the brine, 5 wt % FM, and 30 wt % FM (pH 7.0) solutions, respectively.

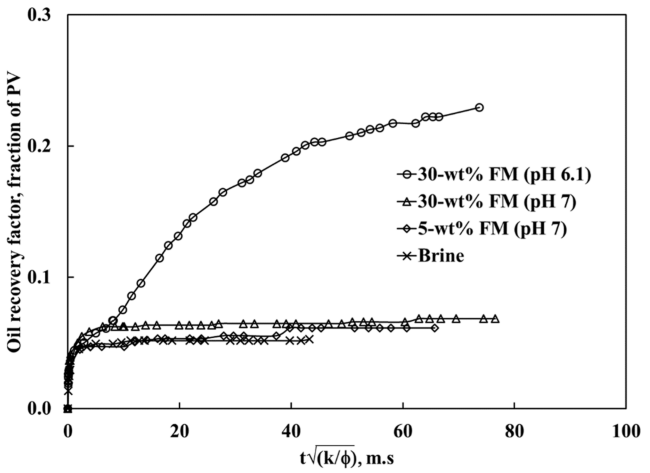

Figure 10. Oil recoveries (in unit of pore volume) from spontaneous imbibition experiments. The 30 wt % FM solution with an initial solution pH of 6.1 gave a markedly different oil recovery from the other three cases. Results are explained in Section 3.2.

Capillary and gravity forces are important for oil recovery during the spontaneous oil displacement by water.[71−74] The relative contribution of these two forces is described by the inverse Bond number, N_B^{-1}.

$$N_B^{-1} = C\frac{\sigma\sqrt{\phi/K}}{\Delta\rho g H} \tag{10}$$

where C is 0.4 for the capillary tube model, σ is the oleic/aqueous phase interfacial tension in N/m, ϕ is porosity, K is permeability in m^2, $\Delta\rho$ is the density difference between the aqueous and oleic phases in kg/m^3, g is the acceleration due to gravity in m/s^2, and H is the height of the core in m. Capillary dominant flow is when $N_B^{-1} > 5$.[75] N_B^{-1} ranged from 7.5 to 67.1 in our displacements (Table 1), indicating capillary dominant flow, as is often the case with core-scale experiments.

To interpret the spontaneous imbibition results, we note that the cores had similar initial water saturations (ranging from 39 to 45%), porosities, and permeabilities. The oil/deionized water IFT at room temperature (22 °C) was measured to be 19.75 mN/m and agreed with the established trend of oil/water IFT by Ramey;[76] hence, we confirmed no chemical contamination of the oil sample used in this research. Table 1 shows the oleic/aqueous phase IFT spectra for the solutions. The oil/brine IFT was lower than the oil/deionized water IFT. This behavior is consistent with many previous studies, in which the oil/brine IFT was significantly affected by brine composition, salinity, and oil composition.[77−83] The result shows that increasing the FM concentration caused a slight reduction in IFT. The 30 wt % FM solutions at different

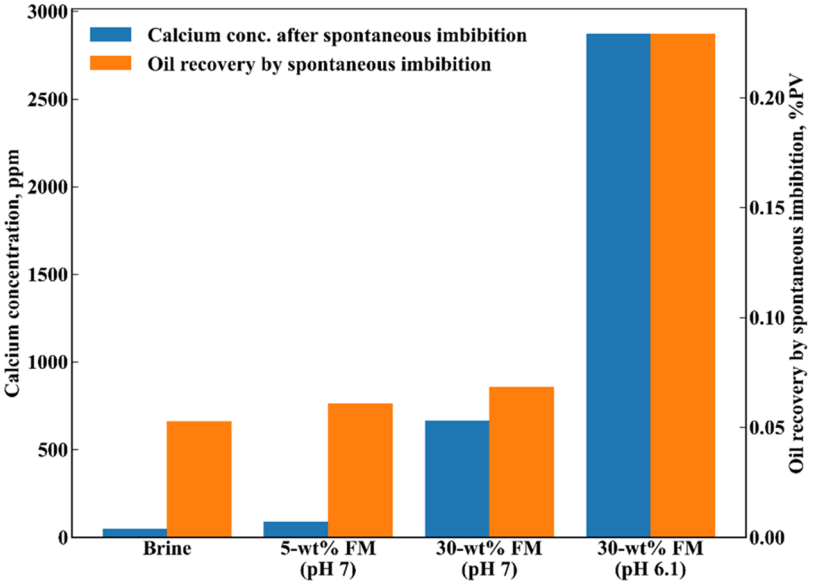

Figure 11. Oil recoveries by spontaneous imbibition and calcium ion concentrations in the solutions after spontaneous imbibition (Section 3.2). The calcium ion concentration increased with the FM concentration. For the pH 7 solutions, however, the oil recoveries during the spontaneous imbibition experiments were quite insensitive to the level of calcite dissolution. The 30 wt % FM solution with an initial solution pH of 6.1 gave a much greater level of calcite dissolution and oil recovery.

https://doi.org/10.1021/acs.energyfuels.3c05081
Energy Fuels XXXX, XXX, XXX−XXX

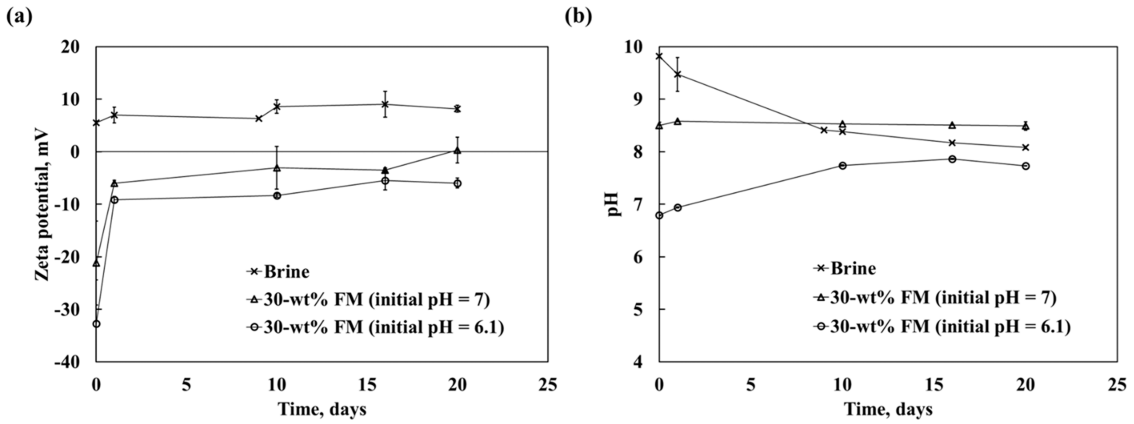

Figure 12. Calcite–water ζ (a) and pH (b) for brine, 30 wt % FM (initial pH = 7), and 30 wt % FM (initial pH = 6.1). The results show that the pH was important for the adsorption of FM. Results are explained in Section 3.2.

initial pH values, 6.1 and 7.0, had similar IFT values but resulted in markedly different oil recoveries (Figure 10). Therefore, the slight IFT reduction with the 30 wt % FM solution (pH 6.1) should not have significantly contributed to the observed oil recovery.

The calcite dissolution experiment (Section 3.1) showed that increasing FM concentration enhanced the level of calcite dissolution, which by itself could be responsible for wettability alteration in carbonates.[84] Figure 11 shows the oil recovery after the spontaneous imbibition process and the respective calcium ion concentration in the solution. As expected, the calcium ion concentration increased with an increasing FM concentration because of the greater level of calcite dissolution. However, the oil recovery was quite insensitive to the level of calcite dissolution for the three FM concentrations at an initial solution pH of 7.0. The 30 wt % FM solution at an initial solution pH of 6.1 yielded a much greater level of calcite dissolution and oil recovery via spontaneous imbibition.

The pH and composition of the aqueous solution affect the ζ of the carbonate surface.[85−90] Numerous LSW studies have shown that the ζ can be correlated with wettability alteration in carbonates.[91−94] Tetteh et al.[95] reported the isoelectric point (IEP) of Indiana limestone rock, which is the point where ζ is equal to zero, to be between pH 7.8 and 8.5. They also showed the IEP to be dependent on brine composition. Figure 12 shows the ζ values of the calcite–water interface in brine, 30 wt % FM (the initial pH 7) and 30 wt % FM (the initial pH 6.1), and the corresponding solution pH over the same time. The ζ value was measured for more than 20 days. Figure 12 shows that the equilibration time had a significant effect on the ζ values, especially for the 30 wt % FM solutions. The ζ of the calcite in brine was positive with an average value of about 8 mV, which is similar to the reported value of ζ in 0.1 M NaCl brine by Song et al.[96] In the 30 wt % FM (initial pH 7) the ζ kept increasing with time and switched polarity from negative to positive after 20 days. In the 30 wt % FM (initial pH 6.1), the ζ was negative throughout the measurement period. For LSW, a negative ζ could develop because of the expansion of the electrical double layer at lower brine ionic strengths, but that is unlikely with high-concentration FM solutions. The reduced ζ by FM is likely a result of the increased level of FM adsorption. The ζ also indicates the charge at the calcite surface; for a positive ζ, the calcite surface of a negative charge results in the relative abundance of positive charge in the interface and vice versa for a negative ζ.

It is not entirely clear how the reduced pH increased the adsorption of FM. One possible explanation is that the increased calcite dissolution at the reduced pH, followed by the adsorption of the Ca^{2+} ion on the rock surface, created more adsorption sites for FM ions. Then, an enhanced level of FM adsorption led to a negative charge. Hence, we hypothesize that the high oil recovery by the 30 wt % FM solution with an initial pH of 6.1 came mainly from the wettability alteration caused synergistically through calcite dissolution, the solution pH, and subsequent geochemical (adsorption and desorption) interactions, leading to a change in surface potential and wettability.

The effect of the wettability change on carbon storage can be quantified from the volume of oil produced in the spontaneous imbibition experiment. By equating the volume of FM solution imbibed with the volume of oil produced, the moles of carbon stored in the core can be estimated. The moles of carbon stored (as a percentage of the moles of carbon in original oil in place) were 0.22, 1.86, and 5.73%, for the 5 wt % FM, 30 wt % FM (initial pH 7), and the 30 wt % FM (initial pH 6.1), respectively. These estimates do not consider the possible displacement of resident brine by the FM solution, which can be significant with the 30 wt % FM solutions because of their large concentration gradients. If the brine in the core was fully displaced by the FM solution, the moles of carbon stored (as a percentage of the moles of carbon in original oil in place) were calculated to be 1.68, 13.82, and 15.44%, for the 5 wt % FM, 30 wt % FM (initial pH 7), and the 30 wt % FM (initial pH = 6.1), respectively. These results show that the wettability alteration can significantly improve carbon storage by FM solution.

Figure 13 shows the total oil recoveries in the Amott experiments (both spontaneous and forced displacements). The oil recoveries at "0 PVI" in this figure are those from spontaneous imbibition. For all of the solutions, the oil recovery leveled off after 5 pore volumes were injected (PVI). The total oil recoveries by the brine, 5 wt % FM, 30 wt % FM (initial pH 7.0), and 30 wt % FM (initial pH 6.1) were 0.41, 0.42, 0.56, and 0.58 PV, respectively.

Table 6 shows the total oil recovery from all of the solutions tested. The 30 wt % FM solution with an initial pH of 7.0 recovered 22.78 mL of oil, and that with an initial pH of 6.1 recovered 24.45 mL in total. They were approximately 90% of the initial amount of oil in the core. However, Figure 13 and Table 6 indicate that they likely had different mechanisms of

https://doi.org/10.1021/acs.energyfuels.3c05081
Energy Fuels XXXX, XXX, XXX−XXX

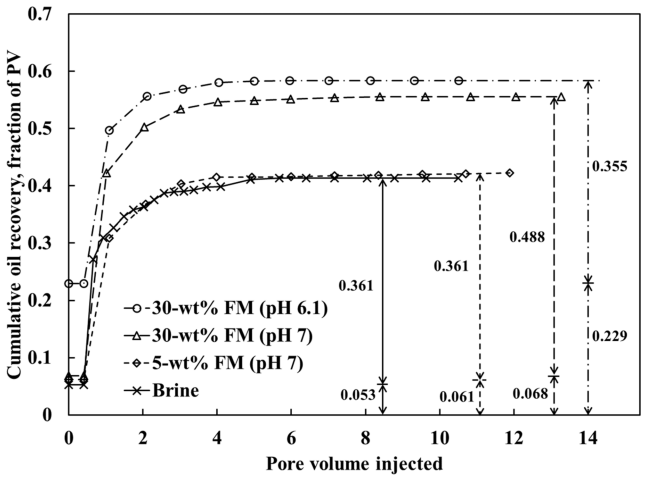

Figure 13. Cumulative oil recoveries from the Amott wettability experiments (both spontaneous and forced displacements) as explained in Section 3.2. The "0 PVI" intercept on the vertical axis corresponds to the oil recovery from the spontaneous imbibition experiment.

Table 6. Amott Indices to Water for All Solutions Tested (Section 3.2)[a]

	oil recovery from spontaneous imbibition		oil recovery from forced imbibition		
case	mL	fraction of PV	mL	fraction of PV	Amott index to water
brine (initial pH 7.0)	2.15	0.053	14.70	0.361	0.1276
5 wt % FM (initial pH 7.0)	2.60	0.061	15.31	0.361	0.1452
30 wt % FM (initial pH 7.0)	2.80	0.068	19.98	0.488	0.1229
30 wt % FM (initial pH 6.1)	9.60	0.229	14.85	0.355	0.3926

[a]The 30 wt% FM solution with an initial pH of 6.1 resulted in a much greater Amott index than the other solutions tested.

oil recovery because the Amott index for the 30 wt % FM solution (pH 6.1) was nearly three times greater than those for the other solutions. The results clearly show that the 30 wt % FM solution (pH 6.1) caused a change in the core wettability, but the 30 wt % FM solution with pH 7.0 did not. This observation highlights the importance of the solution pH in the wettability alteration by an aqueous FM solution. This is consistent with Baghishov et al.,[7] in which the 5 wt % FM solution with an initial pH of 6.1 resulted in wettability alteration of calcite-rich shale, but the straight brine without FM with the same initial pH did not.

As shown in Figure 4, the 30 wt % FM solution with an initial pH of 7.0 dissolved 15.9 times more calcite than the brine in the static calcite dissolution experiments (Section 3.1). The calcite dissolution by the 30 wt % FM (initial pH 7) solution during the forced injection could have increased the permeability of the core. The increased (relative) permeability would increase the capillary number (previously defined in Section 2.2.2) during the injection process, leading to the mobilization of residual oil saturations.

The oil recovery could also have been affected by the in situ pH changes and associated reactions. Figure 14 shows the histories of the effluent pH and average oil saturation during the forced imbibition experiment. Except for the 30 wt % FM solution with an initial pH of 6.1, the effluent pH values were smaller than those recorded from the spontaneous imbibition. For the 30 wt % FM solution with an initial pH of 7.0, the effluent pH increased from its initial value due to calcite dissolution, but did not reach the pH values recorded in the spontaneous imbibition experiment because the equilibrium state was not reached under the dynamic conditions. Therefore, the 30 wt % FM solution with an initial pH of 7.0 could have had similar mechanisms in effect to the other 30 wt % FM solution with an initial pH of 6.1. This implies the potential shortcoming of the Amott wettability test, where the spontaneous and forced displacement may have different solution pH values and ζ. The average oil saturations in the cores injected with the 30 wt % FM solutions were much lower than the 5 wt % FM solution. As mentioned previously, this can be attributed to an increase in capillary number because a substantial level of calcite dissolution could affect the multiphase flow at pore and core scales. Note that FM ions have no impact on oil properties and do not reduce the water–oil IFT to an ultralow value (i.e., 10^{-3} mN/m), unlike specifically formulated surfactant solutions.

The Damköhler number (Da) is a dimensionless number that compares the chemical reaction kinetics and the transport time scale.

$$Da = \frac{kL}{u} \tag{11}$$

where k is the reaction rate constant (in s^{-1}) and u is the average interstitial fluid velocity. The ratio $\frac{L}{u}$ is the residence time of the fluid injected through the core. Increasing the flow rate, u, decreases the residence time, and a smaller residence time reduces the Da. $Da \gg 1$ indicates that reaction kinetics are much faster than the transport rates over the core length under consideration, while $Da < 1$ indicates a transport-controlled process.[97,98] The residence time of the fluid during spontaneous imbibition is much longer than during the forced imbibition stage; hence, $Da_{\text{spontaneous imbibition}} \gg Da_{\text{forced imbibition}}$. Therefore, the spontaneous imbibition stage was reaction-controlled and the forced imbibition stage was transport-controlled. As a result, the Amott wettability index can substantially underestimate the 30 wt% FM solution with an initial pH of 7.0 as a wettability alteration agent for EOR since its oil recovery from carbonate cores is sensitive to the in situ solution pH and ζ. The next section presents the core flood data with the 30 wt% FM solution with an initial pH of 7.0 for investigating its performance under dynamic conditions.

3.3. Core Floods. *3.3.1. Flooding Results.* Figure 15 presents the cumulative oil recovery factors from the core floods with the brine, 20 wt % FM solution, and 30 wt % FM solution, all with an initial pH of 7.0. The water breakthrough occurred at 0.194, 0.221, and 0.229 PVI for the brine, 20 wt % FM, and 30 wt % FM cases, respectively. The oil recovery factor was 38.1% at the water breakthrough for the brine case, 42.2% for the 20 wt % FM case, and 44.0% for the 30 wt % FM case. The final oil recovery factors were nearly the same for the three cases, as expected from the IFT data (Table 1). The two FM solution cases delayed the water breakthrough and improved the displacement efficiency at early times.

For the three core floods: brine, 20 wt % FM, and 30 wt % FM; the pump pressure at the end of core flood was 36, 45,

https://doi.org/10.1021/acs.energyfuels.3c05081
Energy Fuels XXXX, XXX, XXX−XXX

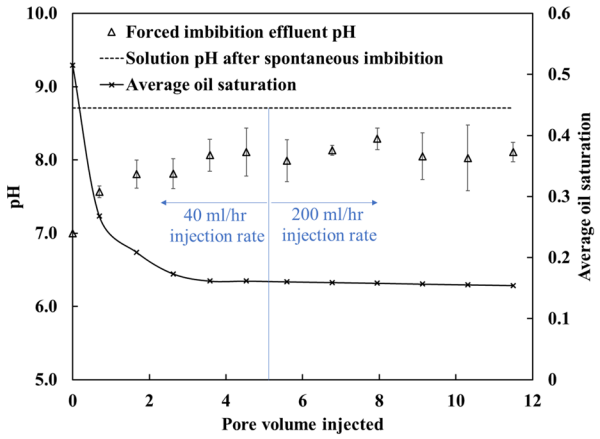

a. 5 wt% FM with an initial pH of 7.0

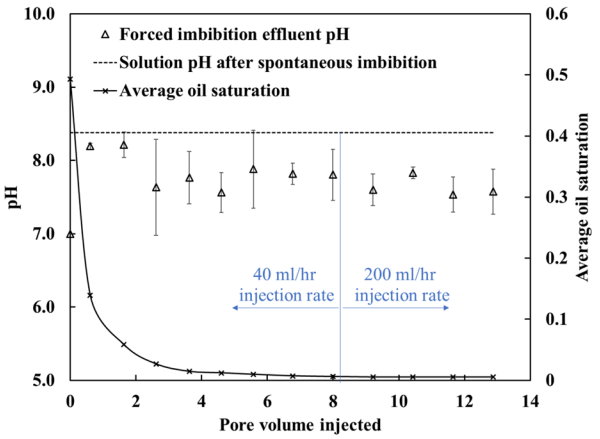

b. 30 wt% FM with an initial pH of 7.0

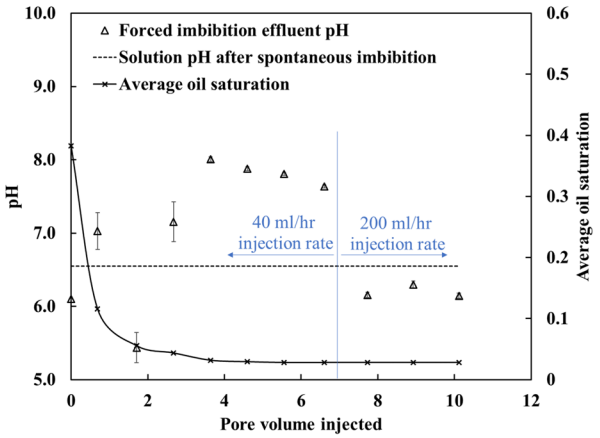

c. 30 wt% FM with an initial pH of 6.1

Figure 14. Effluent pH values from the forced imbibition experiment and the average oil saturation in the cores. Except for the 30 wt % FM solution with an initial pH of 6.1, the effluent pH values were smaller than those of the spontaneous imbibition. Also, when the injection rate was increased, the variation in the effluent pH was much smaller and closer to the initial solution pH.

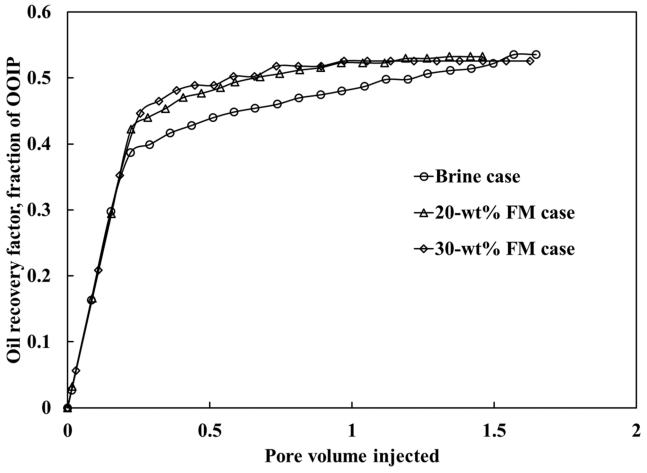

Figure 15. Cumulative oil recovery factors (OOIP) from core floods (Section 3.3.1).

and 70 psi, respectively. Since we used a similar capillary number for the three cases, they should have a similar pressure drop if the wettability status did not change due to FM injection. The increasing injection pressure with an increasing FM concentration indicates a lower water relative permeability, which is consistent with the adjusted relative permeability curve obtained after history matching. As shown in the next subsection, these results were used to quantify the wettability alteration for the two FM solution cases.

3.3.2. History Matching. The oil recoveries from the experiments were history-matched using the relative permeability curves given in Figure 16. The relative permeability was calculated by dividing the effective permeability by oil permeability at initial water saturation in this figure. These relative permeability curves were then used to evaluate the core-scale wettability using the Lak and modified Lak wettability indices.

Table 7 shows these indices calculated based on the history-matched relative permeabilities. Two indices for the brine case had negative values (−0.43 and −0.19); that is, the rock was oil-wet. For the 20 wt % FM case, the Lak wettability index was −0.17 and the modified Lak wettability index was 0.07. These values near zero indicate that the rock was intermediate wet. For the 30 wt % FM case, both wettability indices were positive (i.e., 0.08 and 0.40) and, therefore, the rock was water-wet. This quantitative analysis revealed the extent of the wettability changes after the injection of FM solution toward a more water-wet state. The two indices have a clear positive

https://doi.org/10.1021/acs.energyfuels.3c05081
Energy Fuels XXXX, XXX, XXX−XXX

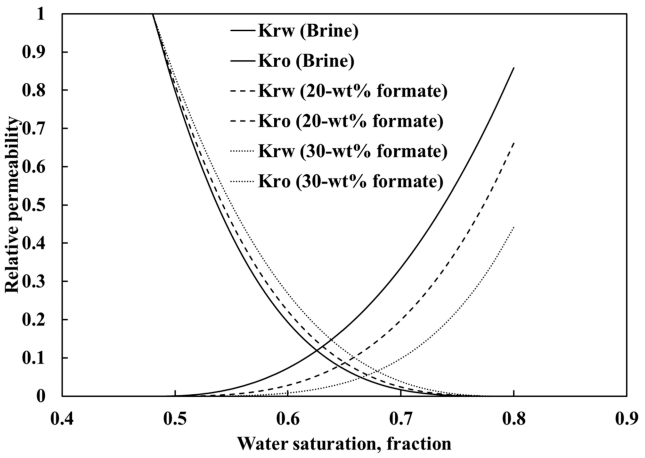

Figure 16. Relative permeability curves obtained from history matching of the core flooding data (Section 3.3.2). Table 7 shows the analysis of these relative permeability curves for the Lak wettability indices.

Table 7. Lak and Modified Lak Wettability Indices Calculated for the Calibrated Relative Permeabilities Using the Core Flooding Data (Section 3.3.2)[a]

	Lak wettability index	modified Lak wettability index
brine	−0.43	−0.19
20 wt % FM	−0.17	0.07
30 wt % FM	0.08	0.40

[a]All solutions had an initial pH of 7.0.

correlation with each other. Note that the viscosities for the three injection solutions were different and properly modeled in the numerical simulations; therefore, the effect of the displacing fluid viscosity on the water breakthrough time was separated from that of wettability alteration in this analysis.

3.3.3. Carbon Storage Calculation. The calibrated simulation models were used to indicate the amount of carbon storage for the core floods with the FM solutions (20 and 30 wt %). As mentioned earlier, FM species in aqueous fluids can act as a carbon carrier for geological carbon storage. A higher concentration of FM solution achieved more uniform displacement, which delayed water breakthrough and increased storage efficiency. In addition, the previous sections discussed that a higher concentration of FM solution altered the wettability of the oil-wet surface through FM adsorption. The adsorption could also be enhanced by a high concentration of FM, but the contribution of FM adsorption was not considered in the current simulation. Using the volume balance, the produced oil volume was equal to the volume of FM solution that was retained in the core. Hence, the following equation gives the carbon amount that replaced the in situ oil:

$$C_j = \frac{V_o \rho_{FM} c_{FM}}{MW} \tag{12}$$

where C_j is the number of moles for the stored carbon as FM, V_o is the produced oil volume, ρ_{FM} is the density of FM solution, c_{FM} is the mass concentration of FM, and MW is the molecular weight of FM. Figure 17 shows that 20 and 30% FM solutions resulted in 4.8 and 8.0% carbon storage (as a percentage of carbon in OOIP), respectively. Note, however, that the reduction in the carbon intensity of oil recovery by injection of FM solution would be different for different initial

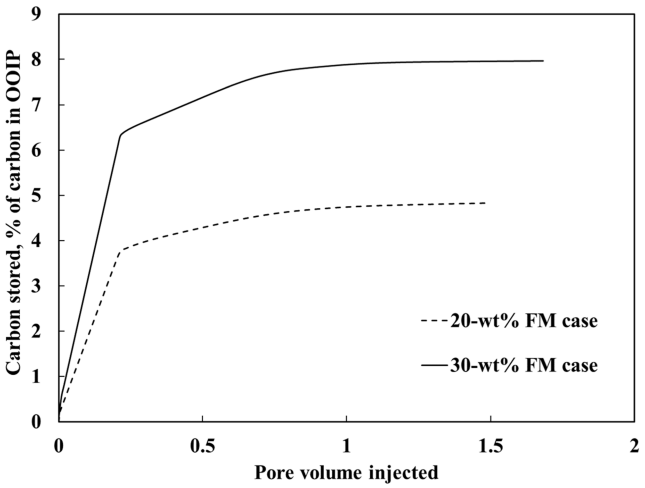

Figure 17. Amount of carbon stored by FM based on the calibrated simulation models for 20 wt % FM and 30 wt % FM solution cases.

water saturations (e.g., secondary and tertiary oil recovery). It is reasonable to consider that part of the resident water would be displaced by the FM solution. For example, if the total volume of produced oil and resident brine were equal to the volume of stored FM solution, 20 and 30% FM solutions would result in 13.1 and 21.5% carbon storage in place of in situ oil, respectively. These results qualitatively indicate a potential of reducing the carbon intensity in waterflooding by FM solution injection.

3.4. Discussion. The local measurements of the contact angle on the calcite chips were conducted as part of this research. However, the results were less conclusive than core-scale data, such as Amott wettability test and core flooding, mainly because the calcite dissolution by the FM solutions led to the effervescence of CO_2 gas bubbles. Various types of variability in surface properties, such as surface roughness and surface heterogeneity, often make contact angle inconclusive as reported in the literature.[99,100] The inherent difficulty of local contact angle measurements was coupled with CO_2 bubbles caused by the calcite dissolution with high-concentration FM solutions in this research. In particular, the effervescence of CO_2 bubbles made it impossible for the oil droplets to adhere to the rock surface when placed in the 30 wt % FM solutions (the initial pH 6.1 and 7.0). The oil films on the oil-aged calcite chips placed in the two 30 wt % FM solutions were completely washed off the surface.

Baghishov et al.[7] proposed that the wettability alteration by FM occurs because of the calcite dissolution caused by a slightly reduced pH and adsorption of FM ions on calcite-rich surfaces. In this research, a substantial level of calcite dissolution was confirmed with the 30 wt % FM solution even at a neutral pH because of the interaction of calcium and FM ions. Then, the reduction in the initial solution pH (from 7.0 to 6.1) substantially enhanced the wettability alteration of the core because the solution pH affected the charge of the calcite surface. The surface charge dictates the adsorption and desorption reactions that occur near the surface. Therefore, the wettability alteration observed in this research can be explained via charge interactions on the calcite surface. As schematically shown in Figure 18, one potential scenario is described below. First, FM imbibition increased calcite dissolution due to the formation of calcium-FM complexes. When the solution pH (e.g., 6.1) was sufficiently below the calcite IEP, the FM ion in

https://doi.org/10.1021/acs.energyfuels.3c05081
Energy Fuels XXXX, XXX, XXX−XXX

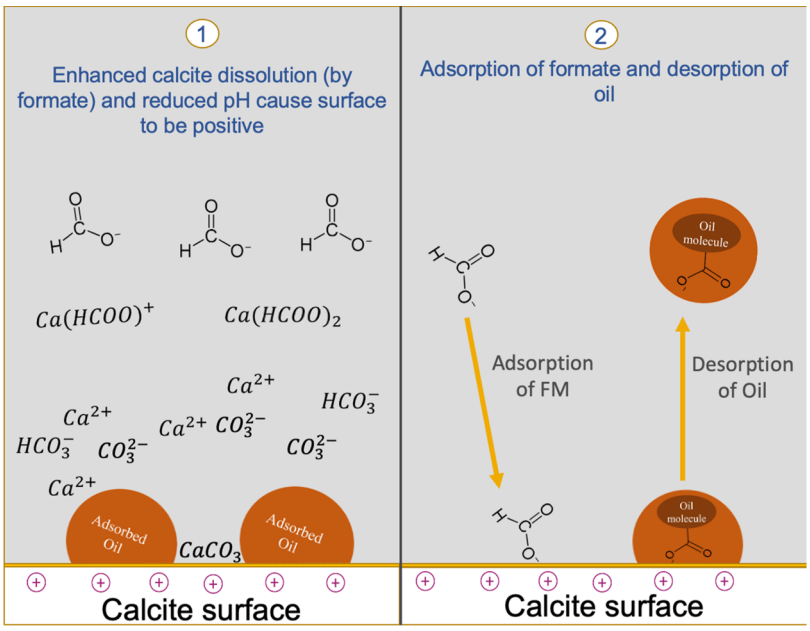

Figure 18. Wettability alteration mechanism by FM in carbonates. The calcite surface is positively charged when the pH is sufficiently lower than the surface IEP. A positively charged calcite surface is likely the key to initiating FM adsorption and the oil desorption process.

the solution adsorbed on the positively charged calcite surface. Then, FM adsorption led to oil desorption from the surface, by increasing the repulsion between the calcite−water and oil−water interface, or by an anion exchange between previously adsorbed oil and FM.

4. CONCLUSIONS

This paper presented a new set of experimental data regarding the core-scale wettability alteration of carbonate porous media with varying concentrations (up to 30 wt %) of FM in NaCl brine. The experiments included Amott wettability tests (spontaneous and forced displacements) and core flooding experiments, along with static calcite dissolution tests. Experimental data were analyzed through geochemical modeling and numerical history matching for a mechanistic understanding of the wettability alteration observed in the experiments. The main conclusions are as follows:

- The static calcite dissolution tests showed that the degree of calcite dissolution increased with increasing FM concentration in the brine, even with an initially neutral pH. For example, the calcium concentration in the 30 wt % FM case was 15.9 times greater than that in the brine case with an initial pH of 7.0. Furthermore, reducing the initial solution pH from 7.0 to 6.1 for the 30 wt % FM solution caused the calcium ion concentration to increase by a factor of 3.2. Geochemical modeling and Raman analysis showed that the increased calcite dissolution could be caused by the interaction between the calcium and FM ions.
- The 30 wt % FM solution with an initial pH of 6.1 yielded 4.7 times greater oil recovery than the brine case in the spontaneous imbibition, resulting in the Amott index of 0.39, which is approximately three times greater than that of the brine case. This clearly indicates the wettability alteration by the FM solution.
- The 30 wt % FM solution with an initial pH of 7.0 yielded only 30% greater oil recovery than the brine case in the spontaneous imbibition; however, it reached nearly the same amount of total oil recovery (spontaneous and forced) as the 30 wt % FM solution with an initial pH of 6.1. Therefore, the Amott index for this case, 0.12, may be misleading since the in situ solution pH was sufficiently lower than the calcite isoelectric point consistently in the forced-imbibition stage, unlike under the static conditions during the spontaneous imbibition stage. Also, the FM-enhanced calcite dissolution could have caused changes in pore structure leading to the mobilization of residual oil.
- Flooding experiments for Indiana limestone cores with FM solutions showed that increasing the FM concentration in the injected solution delayed the water breakthrough. Since FM did not substantially reduce the IFT of the solution with oil, the ultimate oil recovery did not change with the addition of FM into the injection brine. Numerical history matching of the core flooding data showed that increasing the FM concentration in the injected brine rendered the initially oil-wet core to a more water-wet state as quantified by Lak and modified Lak wettability indices.
- The wettability alteration by the 30 wt % FM solution with an initial pH of 7.0 was clear in core flooding experiments, including the forced-displacement part of the Amott wettability test, but unclear under static conditions in the spontaneous imbibition stage of the Amott wettability test. This indicates the importance of in situ solution pH in wettability alteration by aqueous FM solution in carbonate media.

■ ASSOCIATED CONTENT

Supporting Information

The Supporting Information is available free of charge at https://pubs.acs.org/doi/10.1021/acs.energyfuels.3c05081.

Example of PHREEQC input script used for geochemistry modeling of calcite dissolution in FM solution; initial composition of the fluids and initial

https://doi.org/10.1021/acs.energyfuels.3c05081
Energy Fuels XXXX, XXX, XXX−XXX

conditions, additional reactions that were not part of the sit.dat database and had to be included, and the calculated interaction parameters for FM ion (PDF)

AUTHOR INFORMATION

Corresponding Author

Ryosuke Okuno − *Department of Petroleum and Geosystems Engineering, The University of Texas at Austin, Austin, Texas 78712, United States;* orcid.org/0000-0003-3675-1132; Email: okuno@austin.utexas.edu

Authors

Oluwafemi P. Oyenowo − *Department of Petroleum and Geosystems Engineering, The University of Texas at Austin, Austin, Texas 78712, United States;* orcid.org/0000-0001-6209-0636

Hao Wang − *Department of Petroleum and Geosystems Engineering, The University of Texas at Austin, Austin, Texas 78712, United States*

Abouzar Mirzaei-Paiaman − *Department of Petroleum and Geosystems Engineering, The University of Texas at Austin, Austin, Texas 78712, United States;* orcid.org/0000-0001-7350-235X

Omar A. Carrasco-Jaim − *Department of Petroleum and Geosystems Engineering, The University of Texas at Austin, Austin, Texas 78712, United States;* orcid.org/0000-0001-9850-217X

Kai Sheng − *Department of Petroleum and Geosystems Engineering, The University of Texas at Austin, Austin, Texas 78712, United States*

Complete contact information is available at: https://pubs.acs.org/10.1021/acs.energyfuels.3c05081

Notes

The authors declare no competing financial interest.

ACKNOWLEDGMENTS

The authors acknowledge the support of JX Nippon Oil & Gas Exploration for this research along with sponsors of the Energi Simulation Industrial Affiliate Program on Carbon Utilization and Storage (ES Carbon UT) at the Center for Subsurface Energy and the Environment at the University of Texas at Austin. Ryosuke Okuno holds the Pioneer Corporation Faculty Fellowship in the Hildebrand Department of Petroleum and Geosystems Engineering at The University of Texas at Austin.

REFERENCES

(1) IEA. *World Energy Outlook 2022*; IEA: Paris, 2022. https://www.iea.org/reports/world-energy-outlook-2022.

(2) IEA. *Greenhouse Gas Emissions from Energy Data Explorer*; IEA: Paris, 2021. https://www.iea.org/data-and-statistics/data-tools/greenhouse-gas-emissions-from-energy-data-explorer.

(3) Akbar, M.; Vissapragada, B.; Alghamdi, A. H.; et al. A Snapshot of Carbonate Reservoir Evaluation. *Oilfield Rev.* **2000**, *12* (4), 20−21.

(4) Anderson, W. G. Wettability Literature Survey- Part 1: Rock/Oil/Brine Interactions and the Effects of Core Handling on Wettability. *J. Pet. Technol.* **1986**, *38* (10), 1125−1144.

(5) Harimi, B.; Masihi, M.; Mirzaei-Paiaman, A.; Hamidpour, E. Experimental Study of Dynamic Imbibition during Water Flooding of Naturally Fractured Reservoirs. *J. Pet. Sci. Eng.* **2019**, *174*, 1−13.

(6) Morrow, N. R. Wettability and Its Effect on Oil Recovery. *J. Pet. Technol.* **1990**, *42* (12), 1476−1484.

(7) Baghishov, I.; Abeykoon, G. A.; Wang, M.; Oyenowo, O. P.; Argüelles-Vivas, F. J.; Okuno, R. A Mechanistic Comparison of Formate, Acetate, and Glycine as Wettability Modifiers for Carbonate and Shale Formations. *Colloids Surf., A* **2022**, *652*, No. 129849.

(8) Bai, S.; Kubelka, J.; Piri, M. Wettability Alteration by Smart Water Multi-Ion Exchange in Carbonates: A Molecular Dynamics Simulation Study. *J. Mol. Liq.* **2021**, *332*, No. 115830.

(9) Deng, X.; Kamal, M. S.; Patil, S.; Hussain, S. M. S.; Zhou, X. A Review on Wettability Alteration in Carbonate Rocks: Wettability Modifiers. *Energy Fuels* **2020**, *34* (1), 31−54.

(10) Lara Orozco, R. A.; Abeykoon, G. A.; Wang, M.; Argüelles-Vivas, F.; Okuno, R.; Lake, L. W.; Ayirala, S. C.; AlSofi, A. M. Amino Acid as a Novel Wettability Modifier for Enhanced Waterflooding in Carbonate Reservoirs. *SPE Reservoir Eval. Eng.* **2020**, *23* (02), 741−757.

(11) Mahani, H.; Keya, A. L.; Berg, S.; Bartels, W.-B.; Nasralla, R.; Rossen, W. R. Insights into the Mechanism of Wettability Alteration by Low-Salinity Flooding (LSF) in Carbonates. *Energy Fuels* **2015**, *29* (3), 1352−1367.

(12) Standnes, D. C.; Austad, T. Wettability Alteration in Carbonates. *Colloids Surf., A* **2003**, *216* (1−3), 243−259.

(13) Strand, S.; Høgnesen, E. J.; Austad, T. Wettability Alteration of Carbonates—Effects of Potential Determining Ions (Ca2+ and SO42−) and Temperature. *Colloids Surf., A* **2006**, *275* (1−3), 1−10.

(14) Aghajanzadeh, M. R.; Ahmadi, P.; Sharifi, M.; Riazi, M. Wettability Modification of Oil-Wet Carbonate Reservoirs Using Silica-Based Nanofluid: An Experimental Approach. *J. Pet. Sci. Eng.* **2019**, *178*, 700−710.

(15) Ershadi, M.; Alaei, M.; Rashidi, A.; Ramazani, A.; Khosravani, S. Carbonate and Sandstone Reservoirs Wettability Improvement without Using Surfactants for Chemical Enhanced Oil Recovery (C-EOR). *Fuel* **2015**, *153*, 408−415.

(16) Karimi, A.; Fakhroueian, Z.; Bahramian, A.; Pour Khiabani, N.; Darabad, J. B.; Azin, R.; Arya, S. Wettability Alteration in Carbonates Using Zirconium Oxide Nanofluids: EOR Implications. *Energy Fuels* **2012**, *26* (2), 1028−1036.

(17) Naghizadeh, A.; Azin, R.; Osfouri, S.; Fatehi, R. Wettability Alteration of Calcite and Dolomite Carbonates Using Silica Nanoparticles Coated with Fluorine Groups. *J. Pet. Sci. Eng.* **2020**, *188*, No. 106915.

(18) Nazari Moghaddam, R.; Bahramian, A.; Fakhroueian, Z.; Karimi, A.; Arya, S. Comparative Study of Using Nanoparticles for Enhanced Oil Recovery: Wettability Alteration of Carbonate Rocks. *Energy Fuels* **2015**, *29* (4), 2111−2119.

(19) Roustaei, A.; Bagherzadeh, H. Experimental Investigation of SiO2 Nanoparticles on Enhanced Oil Recovery of Carbonate Reservoirs. *J. Pet. Explor. Prod. Technol.* **2015**, *5* (1), 27−33.

(20) Argüelles-Vivas, F. J.; Wang, M.; Abeykoon, G. A.; Okuno, R. Oil Recovery from Fractured Porous Media with/without Initial Water Saturation by Using 3-Pentanone and Its Aqueous Solution. *Fuel* **2020**, *276*, No. 118031.

(21) Lawal, T.; Wang, M.; Abeykoon, G. A.; Argüelles-Vivas, F. J.; Okuno, R. Effect of Chemical Partition Behavior on Oil Recovery by Wettability Alteration in Fractured Tight Reservoirs. *Energy Fuels* **2022**, *36* (2), 797−805.

(22) Wang, M.; Baek, K. H.; Abeykoon, G. A.; Argüelles-Vivas, F. J.; Okuno, R. Comparative Study of Ketone and Surfactant for Enhancement of Water Imbibition in Fractured Porous Media. *Energy Fuels* **2020**, *34* (5), 5159−5167.

(23) Wang, M.; Abeykoon, G. A.; Argüelles-Vivas, F. J.; Okuno, R. Aqueous Solution of 3-Pentanone for Enhanced Oil Production from Tight Porous Media. *J. Pet. Sci. Eng.* **2022**, *213*, No. 110376.

(24) Sohrabi, M.; Riazi, M.; Jamiolahmady, M.; Idah Kechut, N.; Ireland, S.; Robertson, G. Carbonated Water Injection (CWI)−A Productive Way of Using CO2 for Oil Recovery and CO2 Storage. *Energy Procedia* **2011**, *4*, 2192−2199.

(25) Breunig, H. M.; Rosner, F.; Lim, T.-H.; Peng, P. Emerging Concepts in Intermediate Carbon Dioxide Emplacement to Support Carbon Dioxide Removal. *Energy Environ. Sci.* **2023**, *16* (5), 1821−1837.

(26) Oyenowo, O. P.; Sheng, K.; Abeykoon, G. A.; Okuno, R. In *A Case Study of Using Aqueous Formate Solution for Carbon Sequestration and Geological Storage*, The GEOGULF 2021 Conference, October 27−29, 2021, Austin, Texas, GCAGS Transactions, 2021, Vol. 71, pp 203−215.
(27) Oyenowo, O. P.; Sheng, K.; Okuno, R. Simulation Case Studies of Aqueous Formate Solution for Geological Carbon Storage. *Fuel* **2023**, *334*, No. 126643.
(28) Wang, H.; Precious Oyenowo, O.; Okuno, R. Aqueous Formate Solution for Enhanced Water Imbibition in Oil Recovery and Carbon Storage in Carbonate Reservoirs. *Fuel* **2023**, *345*, No. 128198.
(29) Downs, J. D. Formate Brines: Novel Drilling and Completion Fluids for Demanding Environments. In *SPE International Symposium on Oilfield Chemistry* New Orleans, Louisiana, 1993.
(30) Liu, Q.; Wu, L.; Gülak, S.; Rockstroh, N.; Jackstell, R.; Beller, M. Towards a Sustainable Synthesis of Formate Salts: Combined Catalytic Methanol Dehydrogenation and Bicarbonate Hydrogenation. *Angew. Chem. Int. Ed* **2014**, *53* (27), 7085−7088.
(31) Hietala, J.; Vuori, A.; Johnsson, P.; Pollari, I.; Reutemann, W.; Kieczka, H. Formic Acid. In *Ullmann's Encyclopedia of Industrial Chemistry*; Wiley-VCH, Ed.; Wiley, 2016; pp 1−22.
(32) Xu, D.; Li, K.; Jia, B.; Sun, W.; Zhang, W.; Liu, X.; Ma, T. Electrocatalytic CO_2 Reduction towards Industrial Applications. *Carbon Energy* **2023**, *5* (1), No. e230.
(33) Agarwal, A. S.; Zhai, Y.; Hill, D.; Sridhar, N. The Electrochemical Reduction of Carbon Dioxide to Formate/Formic Acid: Engineering and Economic Feasibility. *ChemSusChem* **2011**, *4* (9), 1301−1310.
(34) Fernández-Caso, K.; Díaz-Sainz, G.; Alvarez-Guerra, M.; Irabien, A. Electroreduction of CO_2: Advances in the Continuous Production of Formic Acid and Formate. *ACS Energy Lett.* **2023**, *8* (4), 1992−2024.
(35) Philips, M. F.; Gruter, G.-J. M.; Koper, M. T. M.; Schouten, K. J. P. Optimizing the Electrochemical Reduction of CO_2 to Formate: A State-of-the-Art Analysis. *ACS Sustainable Chem. Eng.* **2020**, *8* (41), 15430−15444.
(36) Xiang, H.; Miller, H. A.; Bellini, M.; Christensen, H.; Scott, K.; Rasul, S.; Yu, E. H. Production of Formate by CO_2 Electrochemical Reduction and Its Application in Energy Storage. *Sustainable Energy Fuels* **2020**, *4* (1), 277−284.
(37) Zhang, S.; Kang, P.; Meyer, T. J. Nanostructured Tin Catalysts for Selective Electrochemical Reduction of Carbon Dioxide to Formate. *J. Am. Chem. Soc.* **2014**, *136* (5), 1734−1737.
(38) Zheng, X.; De Luna, P.; García De Arquer, F. P.; Zhang, B.; Becknell, N.; Ross, M. B.; Li, Y.; Banis, M. N.; Li, Y.; Liu, M.; Voznyy, O.; Dinh, C. T.; Zhuang, T.; Stadler, P.; Cui, Y.; Du, X.; Yang, P.; Sargent, E. H. Sulfur-Modulated Tin Sites Enable Highly Selective Electrochemical Reduction of CO2 to Formate. *Joule* **2017**, *1* (4), 794−805.
(39) Gao, T.; Xia, B.; Yang, K.; Li, D.; Shao, T.; Chen, S.; Li, Q.; Duan, J. Techno-Economic Analysis and Carbon Footprint Accounting for Industrial CO_2 Electrolysis Systems. *Energy Fuels* **2023**, *37* (23), 17997−18008.
(40) Ramdin, M.; Morrison, A. R. T.; De Groen, M.; Van Haperen, R.; De Kler, R.; Irtem, E.; Laitinen, A. T.; Van Den Broeke, L. J. P.; Breugelmans, T.; Trusler, J. P. M.; Jong, W. D.; Vlugt, T. J. H. High-Pressure Electrochemical Reduction of CO_2 to Formic Acid/Formate: Effect of pH on the Downstream Separation Process and Economics. *Ind. Eng. Chem. Res.* **2019**, *58* (51), 22718−22740.
(41) OCOchem, Technology. https://ocochem.com/technology/ (accessed Sept 27, 2023).
(42) European Commission CORDIS. Oxalic Acid from CO_2 Using Electrochemistry at Demonstration scale. (May 26, 2022) DOI: 10.3030/767798.
(43) Howard, S. K. Formate Brines for Drilling and Completion: State of the Art. In *SPE Annual Technical Conference and Exhibition* Dallas, Texas, 1995.
(44) Lake, L.; Johns, R. T.; Rossen, W. R.; Pope, G. A. *Fundamentals of Enhanced Oil Recovery*; Society of Petroleum Engineers, 2014.
(45) Rapoport, L. A.; Leas, W. J. Properties of Linear Waterfloods. *J. Pet. Technol.* **1953**, *5* (05), 139−148.
(46) Skoog, D. A.; Holler, F. J.; Crouch, S. R. *Principles of Instrumental Analysis*, 7th ed.; Cengage Learning, 2018.
(47) Parkhurst, D. L.; Appelo, C. A. J. *Description of Input and Examples for PHREEQC version 3—A Computer Program for Speciation, Batch-reaction, One-dimensional Transport, and Inverse Geochemical Calculations*; U.S. Geological Survey Techniques and Methods, 2013.
(48) Clegg, S. L. Activity coefficients in natural waters. In *Activity Coefficients in Electrolyte Solutions*; CRC Press, 2018; pp 279−434.
(49) Pitzer, K. S. *Activity Coefficients in Electrolyte Solutions*; CRC Press, 1991.
(50) Bretti, C.; Foti, C.; Sammartano, S. A New Approach in the Use of SIT in Determining the Dependence on Ionic Strength of Activity Coefficients. Application to Some Chloride Salts of Interest in the Speciation of Natural Fluids. *Chem. Speciation Bioavailability* **2004**, *16* (3), 105−110.
(51) Bretti, C.; Foti, C.; Porcino, N.; Sammartano, S. SIT Parameters for 1:1 Electrolytes and Correlation with Pitzer Coefficients. *J. Solution Chem.* **2006**, *35* (10), 1401−1415.
(52) Crea, F.; Foti, C.; De Stefano, C.; Sammartano, S. Sit Parameters for 1:2 Electrolytes and Correlation with Pitzer Coefficients. *Ann. Chim.* **2007**, *97* (1−2), 85−95.
(53) Loos, D.; Pasel, C.; Luckas, M.; Schmidt, K. G.; Herbell, J.-D. Experimental Investigation and Modelling of the Solubility of Calcite and Gypsum in Aqueous Systems at Higher Ionic Strength. *Fluid Phase Equilib.* **2004**, *219* (2), 219−229.
(54) Carrell, C. J.; Carrell, H. L.; Erlebacher, Jonah.; Glusker, J. P. Structural Aspects of Metal Ion Carboxylate Interactions. *J. Am. Chem. Soc.* **1988**, *110* (26), 8651−8656.
(55) Martinek, T.; Duboué-Dijon, E.; Timr, Š.; Mason, P. E.; Baxová, K.; Fischer, H. E.; Schmidt, B.; Pluhařová, E.; Jungwirth, P. Calcium Ions in Aqueous Solutions: Accurate Force Field Description Aided by *Ab Initio* Molecular Dynamics and Neutron Scattering. *J. Chem. Phys.* **2018**, *148* (22), No. 222813.
(56) Nguyen, P. T. M.; Nguyen, V. T.; Annapureddy, H. V. R.; Dang, L. X.; Do, D. D. Thermodynamics and Kinetics of Na+/K+-Formate Ion Pairs Association in Polarizable Water: A Molecular Dynamics Study. *Chem. Phys. Lett.* **2012**, *554*, 90−95.
(57) Shock, E. L.; Koretsky, C. M. Metal-Organic Complexes in Geochemical Processes: Estimation of Standard Partial Molal Thermodynamic Properties of Aqueous Complexes between Metal Cations and Monovalent Organic Acid Ligands at High Pressures and Temperatures. *Geochim. Cosmochim. Acta* **1995**, *59* (8), 1497−1532.
(58) Computer Modelling Group. *IMEX Version 2020 User's Guide*; Computer Modelling Group: Calgary, Alberta, Canada, 2020.
(59) Alarji, H.; Alazman, A.; Regenauer-Lieb, K. The Impact of Effective Tortuosity on Carbonate Acidizing and the Validation of Damköhler and Péclet Dimensionless Phase Space. *J. Pet. Sci. Eng.* **2022**, *212*, No. 110313.
(60) Churcher, P. L.; French, P. R.; Shaw, J. C.; Schramm, L. L. Rock Properties of Berea Sandstone, Baker Dolomite, and Indiana Limestone. In *SPE International Symposium on Oilfield Chemistry* Anaheim, California, 1991.
(61) Elkhoury, J. E.; Shankar, R.; Ramakrishnan, T. S. Resolution and Limitations of X-Ray Micro-CT with Applications to Sandstones and Limestones. *Transp Porous Med.* **2019**, *129* (1), 413−425.
(62) Lipovetsky, T.; Zhuang, L.; Teixeira, W. G.; Boyd, A.; May Pontedeiro, E.; Moriconi, L.; Alves, J. L. D.; Couto, P.; Van Genuchten, M. Th. HYPROP Measurements of the Unsaturated Hydraulic Properties of a Carbonate Rock Sample. *J. Hydrol.* **2020**, *591*, No. 125706.
(63) Mirzaei-Paiaman, A. New Methods for Qualitative and Quantitative Determination of Wettability from Relative Permeability Curves: Revisiting Craig's Rules of Thumb and Introducing Lak Wettability Index. *Fuel* **2021**, *288*, No. 119623.

https://doi.org/10.1021/acs.energyfuels.3c05081
Energy Fuels XXXX, XXX, XXX−XXX

(64) Mirzaei-Paiaman, A.; Faramarzi-Palangar, M.; Djezzar, S.; Kord, S. A New Approach to Measure Wettability by Relative Permeability Measurements. *J. Pet. Sci. Eng.* **2022**, *208*, No. 109191.
(65) Rudolph, W. W.; Irmer, G. Raman Spectroscopic Studies on Aqueous Sodium Formate Solutions and DFT Calculations. *J. Solution Chem.* **2022**, *51* (8), 935−961.
(66) Chukanov, N. V.; Menor-Salvan, C.; Gurzhiy, V. V.; Izatulina, A. R.; Pekov, I. V.; Vigasina, M. F.; Ksenofontov, D. A.; Britvin, S. N. Biogenic Orthorhombic α-Calcium Formate from Sediments of Alkali Lake, Oregon, USA. *Minerals* **2021**, *11* (5), 448.
(67) Weaver, J.; Soderquist, C. Z.; Washton, N. M.; Lipton, A. S.; Gassman, P. L.; Lukens, W. W.; Kruger, A. A.; Wall, N. A.; McCloy, J. S. Chemical Trends in Solid Alkali Pertechnetates. *Inorg. Chem.* **2017**, *56* (5), 2533−2544.
(68) Mason, G.; Morrow, N. R. Developments in Spontaneous Imbibition and Possibilities for Future Work. *J. Pet. Sci. Eng.* **2013**, *110*, 268−293.
(69) Mirzaei-Paiaman, A.; Masihi, M. Scaling Equations for Oil/Gas Recovery from Fractured Porous Media by Counter-Current Spontaneous Imbibition: From Development to Application. *Energy Fuels* **2013**, *27* (8), 4662−4676.
(70) Mirzaei-Paiaman, A.; Kord, S.; Hamidpour, E.; Mohammadzadeh, O. Scaling One- and Multi-Dimensional Co-Current Spontaneous Imbibition Processes in Fractured Reservoirs. *Fuel* **2017**, *196*, 458−472.
(71) Gupta, R.; Mohanty, K. Temperature Effects on Surfactant-Aided Imbibition Into Fractured Carbonates. *SPE J.* **2010**, *15* (03), 588−597.
(72) Meng, Q.; Liu, H.; Wang, J.; Pang, Z. Effect of Gravity on Spontaneous Imbibition from Cores with Two Ends Open in the Frontal Flow Period. *J. Pet. Sci. Eng.* **2016**, *141*, 16−23.
(73) Mirzaei-Paiaman, A. Analysis of Counter-Current Spontaneous Imbibition in Presence of Resistive Gravity Forces: Displacement Characteristics and Scaling. *Journal of Unconventional Oil and Gas Resources* **2015**, *12*, 68−86.
(74) Rostami Ravari, R.; Strand, S.; Austad, T. Combined Surfactant-Enhanced Gravity Drainage (SEGD) of Oil and the Wettability Alteration in Carbonates: The Effect of Rock Permeability and Interfacial Tension (IFT). *Energy Fuels* **2011**, *25* (5), 2083−2088.
(75) Schechter, D. S.; Zhou, D.; Orr, F. M. Low IFT Drainage and Imbibition. *J. Pet. Sci. Eng.* **1994**, *11* (4), 283−300.
(76) Ramey, Jr, H. J. *Correlations of Surface and Interfacial Tensions of Reservoir Fluids*; Society of Petroleum Engineers, 1973.
(77) Lashkarbolooki, M.; Ayatollahi, S. The Effects of pH, Acidity, Asphaltene and Resin Fraction on Crude Oil/Water Interfacial Tension. *J. Pet. Sci. Eng.* **2018**, *162*, 341−347.
(78) Mehraban, M. F.; Farzaneh, S. A.; Sohrabi, M. Debunking the Impact of Salinity on Crude Oil/Water Interfacial Tension. *Energy Fuels* **2021**, *35* (5), 3766−3779.
(79) Moeini, F.; Hemmati-Sarapardeh, A.; Ghazanfari, M.-H.; Masihi, M.; Ayatollahi, S. Toward Mechanistic Understanding of Heavy Crude Oil/Brine Interfacial Tension: The Roles of Salinity, Temperature and Pressure. *Fluid Phase Equilib.* **2014**, *375*, 191−200.
(80) Nowrouzi, I.; Manshad, A. K.; Mohammadi, A. H. Effects of Dissolved Binary Ionic Compounds and Different Densities of Brine on Interfacial Tension (IFT), Wettability Alteration, and Contact Angle in Smart Water and Carbonated Smart Water Injection Processes in Carbonate Oil Reservoirs. *J. Mol. Liq.* **2018**, *254*, 83−92.
(81) Rostami, P.; Mehraban, M. F.; Sharifi, M.; Dejam, M.; Ayatollahi, S. Effect of Water Salinity on Oil/Brine Interfacial Behaviour during Low Salinity Waterflooding: A Mechanistic Study. *Petroleum* **2019**, *5* (4), 367−374.
(82) Soleymanzadeh, A.; Rahmati, A.; Yousefi, M.; Roshani, B. Theoretical and Experimental Investigation of Effect of Salinity and Asphaltene on IFT of Brine and Live Oil Samples. *J. Pet. Explor. Prod. Technol.* **2021**, *11* (2), 769−781.
(83) Zhu, D.; Li, B.; Li, H.; Li, B.; Cao, Y.; Li, Z. Effects of Low-Salinity Water on the Interface Characteristics and Imbibition Process. *J. Pet. Sci. Eng.* **2022**, *208*, No. 109564.
(84) Hiorth, A.; Cathles, L. M.; Madland, M. V. The Impact of Pore Water Chemistry on Carbonate Surface Charge and Oil Wettability. *Transp Porous Med.* **2010**, *85* (1), 1−21.
(85) Al Mahrouqi, D.; Vinogradov, J.; Jackson, M. D. Zeta Potential of Artificial and Natural Calcite in Aqueous Solution. *Adv. Colloid Interface Sci.* **2017**, *240*, 60−76.
(86) Heberling, F.; Klačić, T.; Raiteri, P.; Gale, J. D.; Eng, P. J.; Stubbs, J. E.; Gil-Díaz, T.; Begović, T.; Lützenkirchen, J. Structure and Surface Complexation at the Calcite(104)−Water Interface. *Environ. Sci. Technol.* **2021**, *55* (18), 12403−12413.
(87) Leroy, P.; Maineult, A.; Li, S.; Vinogradov, J. The Zeta Potential of Quartz. Surface Complexation Modelling to Elucidate High Salinity Measurements. *Colloids Surf., A* **2022**, *650*, No. 129507.
(88) Somasundaran, P.; Agar, G. E. The Zero Point of Charge of Calcite. *J. Colloid Interface Sci.* **1967**, *24* (4), 433−440.
(89) Vinogradov, J.; Hidayat, M.; Sarmadivaleh, M.; Derksen, J.; Vega-Maza, D.; Iglauer, S.; Jougnot, D.; Azaroual, M.; Leroy, P. Predictive Surface Complexation Model of the Calcite-Aqueous Solution Interface: The Impact of High Concentration and Complex Composition of Brines. *J. Colloid Interface Sci.* **2022**, *609*, 852−867.
(90) Zeng, L.; Chen, Y.; Lu, Y.; Hossain, M. M.; Saeedi, A.; Xie, Q. Role of Brine Composition on Rock Surface Energy and Its Implications for Subcritical Crack Growth in Calcite. *J. Mol. Liq.* **2020**, *303*, No. 112638.
(91) Jackson, M. D.; Al-Mahrouqi, D.; Vinogradov, J. Zeta Potential in Oil-Water-Carbonate Systems and Its Impact on Oil Recovery during Controlled Salinity Water-Flooding. *Sci. Rep.* **2016**, *6* (1), No. 37363, DOI: 10.1038/srep37363.
(92) Zhang, P.; Austad, T. Wettability and Oil Recovery from Carbonates: Effects of Temperature and Potential Determining Ions. *Colloids Surf., A* **2006**, *279* (1−3), 179−187.
(93) Alshakhs, M. J.; Kovscek, A. R. Understanding the Role of Brine Ionic Composition on Oil Recovery by Assessment of Wettability from Colloidal Forces. *Adv. Colloid Interface Sci.* **2016**, *233*, 126−138.
(94) Tetteh, J. T.; Barimah, R.; Korsah, P. K. Ionic Interactions at the Crude Oil−Brine−Rock Interfaces Using Different Surface Complexation Models and DLVO Theory: Application to Carbonate Wettability. *ACS Omega* **2022**, *7* (8), 7199−7212.
(95) Tetteh, J. T.; Alimoradi, S.; Brady, P. V.; Barati Ghahfarokhi, R. Electrokinetics at Calcite-Rich Limestone Surface: Understanding the Role of Ions in Modified Salinity Waterflooding. *J. Mol. Liq.* **2020**, *297*, No. 111868.
(96) Song, J.; Zeng, Y.; Wang, L.; Duan, X.; Puerto, M.; Chapman, W. G.; Biswal, S. L.; Hirasaki, G. J. Surface Complexation Modeling of Calcite Zeta Potential Measurements in Brines with Mixed Potential Determining Ions (Ca2+, CO32−, Mg2+, SO42−) for Characterizing Carbonate Wettability. *J. Colloid Interface Sci.* **2017**, *506*, 169−179.
(97) Akindipe, D.; Saraji, S.; Piri, M. Pore Matrix Dissolution in Carbonates: An in-Situ Experimental Investigation of Carbonated Water Injection. *Appl. Geochem.* **2022**, *147*, No. 105483.
(98) Steefel, C. I.; Maher, K. Fluid-Rock Interaction: A Reactive Transport Approach. *Rev. Mineral. Geochem.* **2009**, *70* (1), 485−532.
(99) Chau, T. T.; Bruckard, W. J.; Koh, P. T. L.; Nguyen, A. V. A Review of Factors That Affect Contact Angle and Implications for Flotation Practice. *Adv. Colloid Interface Sci.* **2009**, *150* (2), 106−115.
(100) Kung, C. H.; Sow, P. K.; Zahiri, B.; Mérida, W. Assessment and Interpretation of Surface Wettability Based on Sessile Droplet Contact Angle Measurement: Challenges and Opportunities. *Adv. Mater. Interfaces* **2019**, *6* (18), No. 1900839.
(101) Anderson, G. M. *Thermodynamics of Natural Systems*; Cambridge University Press, 2005.
(102) Wagman, D. D.; Evans, W. H.; Parker, V. B.; Schumm, R. H.; Halow, I.; Bailey, S. M.; Churney, K. L.; Nuttall, R. L.The NBS tables of chemical thermodynamic properties. Selected values for inorganic and C_1 and C_2 organic substances in SI units *J. Phys. Chem. Ref. Data* 1982; *11*2https://srd.nist.gov/JPCRD/jpcrdS2Vol11.pdf.

https://doi.org/10.1021/acs.energyfuels.3c05081
Energy Fuels XXXX, XXX, XXX−XXX